

Counterpart of the Chandrasekhar-Kendall state in noncentrosymmetric superconductors

Julien Garaud,^{1,*} Anatolii Korneev,² Albert Samoilenka,³
Alexander Molochkov,² Egor Babaev,³ and Maxim Chernodub^{1,†}

¹*Institut Denis Poisson CNRS/UMR 7013, Université de Tours, 37200 France*

²*Pacific Quantum Center, Far Eastern Federal University, Sukhanova 8, Vladivostok, 690950, Russia*

³*Department of Physics, Royal Institute of Technology, SE-106 91 Stockholm, Sweden*

(Dated: July 20, 2023)

We demonstrate that superconductors with broken inversion symmetry support a family of stable, spatially localized configurations of the self-knotted magnetic field. These solutions, that we term “toroflux,” are the superconducting counterparts of the Chandrasekhar-Kendall states (spheromaks) that appear in highly conducting, force-free astrophysical and nuclear-fusion plasmas. The superconducting torofluxes are solutions of superconducting models, in the presence of a parity-breaking Lifshitz invariant associated with the O point-group symmetry. These solutions are characterized by a non-vanishing helicity of the magnetic field, and also by a toroidal dipole moment of the magnetic field. We demonstrate that a magnetic dipole or a ferromagnetic inclusion in the bulk of a noncentrosymmetric superconductor sources finite-energy toroflux solutions.

I. INTRODUCTION

Ordinary type-2 superconductors expel weak magnetic fields due to the Meissner effect, while at elevated fields the magnetic flux penetrates in the form of a lattice or a liquid of vortices (see, *e.g.*, [1]). Moreover, quantum or thermal fluctuations can induce closed loops of such quantum vortices. Because of the vortex string tension, these loops are unstable, and eventually decay. Thus, apart from certain cases demonstrated in multicomponent systems that allow different topology [2] bulk superconductors do not feature stable, localized configurations of the magnetic field (in three dimensions). In this paper, we demonstrate that bulk noncentrosymmetric superconductors feature a class of localized, impurity-induced, configurations of a knotted magnetic field. We coin these solutions “toroflux,” since the geometry of their current and flux lines resemble a popular toroflux toy [3].

Noncentrosymmetric superconductors, that is superconductors whose crystal lattices lack inversion symmetry, have attracted significant attention from both theoretical [4–9] and experimental [10–14] communities. A key property of a noncentrosymmetric crystal is that it cannot be superimposed on its spatially inverted image with the help of spatial translations. The crystal thus breaks explicitly the parity inversion group. Since the superconducting order parameter captures the parity-breaking properties of the underlying ionic lattice, the noncentrosymmetric superconductors constitute a class of exotic systems that spontaneously breaks a continuous symmetry, in a parity-violating medium (see, *e.g.*, Refs. [15–17] for detailed reviews). Ginzburg-Landau free energies of noncentrosymmetric superconductors include contributions that are linear in the magnetic field and in the gradients of the superconducting order parameter: $\propto k_{ij} B_i \text{Im}(\psi^* D_j \psi)$. Here \mathbf{D} is the gauge derivative of the order parameter ψ , and k_{ij} are coefficients that depend on the crystal symmetry. In this work, we consider

a particular class of noncentrosymmetric superconductors with chiral octahedral O symmetry.

Parity-breaking superconducting systems feature several distinctive properties: they generate unusual magnetoelectric transport phenomena, exhibit a correlation between supercurrents and electron spin polarizations, lead to the emergence of helical states, and host, in the background of the magnetic field, the vortex lattices with exotic spatial structure [15–18]. Notably, vortices in these superconducting materials can exhibit an inversion of the magnetic field at a certain distance from the vortex core [19, 20]. This property leads to non-monotonic inter-vortex forces and thus to the formation of vortex-vortex bound states, vortex clusters, and nontrivial bound states at the boundary of the sample [19, 20]. The parity breaking in noncentrosymmetric superconductors can also modify the Josephson effect with an unconventional, phase-shifted relation for the Josephson current [21, 22]. Linked by a uniaxial ferromagnet, the unconventional Josephson junction was suggested to serve as an element of a qubit with a simple and presumably robust architecture [23].

The toroflux solutions that we find in this paper, are the counterparts of the Chandrasekhar-Kendall states [24], in the context of noncentrosymmetric superconductors. The Chandrasekhar-Kendall states are the divergence-free eigenvectors of the curl operator that determine the minimum-energy equilibrium configurations in magnetohydrodynamics of highly conducting plasmas. These states appear in various physical contexts, ranging from astrophysical plasmas [24] to the nuclear fusion theory [25]. In the latter case, the Chandrasekhar-Kendall eigenvectors are also known as Taylor states [25], which represent the relaxed minimum energy states of a plasma in a spheromak device (*i.e.*, inside a spherical shell that confines the plasma) [26, 27]. The principal difference between the toroflux state in parity-broken superconductors and the Chandrasekhar-Kendall state in a conduct-

ing plasma is that the toroflux are strongly localized configurations. The spatial localization of both the magnetic field and the supercurrent of the toroflux originates from the Meissner effect.

Our torofluxes are eigenstates of the London equations for a noncentrosymmetric superconducting material. Labeled by their orbital ($0 < l < \infty$) and magnetic ($-l \leq m \leq +l$) quantum numbers, there are infinitely many (l, m) toroflux modes, for a given value of the parity-breaking parameter. All of the toroflux modes have an intrinsic divergence at the origin, and therefore they require a regularization at the core of the solutions. We demonstrate that each divergent mode is regularized by (pointlike) magnetic multipole sources. The case of a pointlike magnetic dipole is of particular physical relevance, as it corresponds to magnetic impurities inside a noncentrosymmetric superconductor. We argue that such magnetic impurities systematically induce an $(l, m) = (1, 0)$ toroflux mode.

The superconducting toroflux solutions found in this paper share some similarities with knotted field configurations that appear in many areas of physics, including particle physics [28], condensed matter [2, 29–31], and the classical field theory [32, 33]. Knotted electromagnetic field configurations were also suggested to play a role in the chirally imbalanced quark-gluon plasmas [34–38].

The paper is organized as follows. In Sec. II, we introduce the Ginzburg-Landau theory for parity-breaking superconductors and derive the corresponding classical equations in the London limit. In Sec. III, we express the London equation in terms of a force-free field and discuss localized solutions for the magnetic field and electric currents, using the basis of vector spherical harmonics. There, we also determine the energy and helicity densities for the infinite tower of toroflux states. We further demonstrate that in the London limit, the total energy of the solution diverges in its core. Next, in Sec. IV, we show that a ferromagnetic inclusion regularizes the singular behavior of the solution, serving, at the same time, as a source for a finite-energy superconducting toroflux. Finally, in Sec. V we investigate the case where the inclusion is a ferromagnetic dipole. There, we explicitly construct the toroflux solutions sourced by such an impurity. We discuss their properties and, in particular, the influence of the parity-breaking parameter on the structure, energy, and helicity of the toroflux solutions. Our conclusions are presented in the last section.

II. THEORETICAL FRAMEWORK

A. Parity-broken formulation

We consider a class of isotropic noncentrosymmetric superconductors that are invariant under spatial rotations while possessing, at the same time, an explicitly broken discrete group of spatial inversions. The macro-

scopic physics of these materials may be described within the Ginzburg-Landau theory supplemented with the Lifshitz term of the simplest form $\mathbf{j} \cdot \mathbf{B}$ that directly couples the magnetic field \mathbf{B} to a current \mathbf{j} expressed via the superconducting order parameter ψ (for a review, see Refs. [15, 39]). This particular structure of the Lifshitz term describes a class of the noncentrosymmetric superconductors with an O -point group symmetry such as, for example, $\text{Li}_2\text{Pt}_3\text{B}$ [12, 40], $\text{Mo}_3\text{Al}_2\text{C}$ [41, 42], and PtSbS [43].

In the vicinity of the superconducting critical temperature, the density \mathcal{F} of the Ginzburg-Landau free energy $F = \int d^3x \mathcal{F}$ can be written as follows:

$$\mathcal{F} = \frac{\mathbf{B}^2}{8\pi} + \frac{k}{2} \sum_{a=\pm} |\mathcal{D}_a \psi|^2 + \frac{\beta}{2} (|\psi|^2 - \psi_0^2)^2, \quad (1a)$$

$$\text{where } \mathcal{D}_{\pm} := \nabla - ie\mathbf{A} + ie\kappa_{\pm}\mathbf{B}. \quad (1b)$$

The single-component order parameter $\psi = |\psi|e^{i\varphi}$ stands for the density of Cooper pairs. The gauge derivative \mathcal{D} couples the scalar field ψ to the vector potential \mathbf{A} and the magnetic field $\mathbf{B} = \nabla \times \mathbf{A}$. The coefficients of the Ginzburg-Landau model (1), including the parity-breaking couplings $\kappa_{\pm} = \chi \pm \nu$, can be expressed in terms of the parameters of the microscopic model [20] (see also [44]). In the microscopic single-particle Hamiltonian, the parity-odd terms originate from the antisymmetric spin-orbit couplings $\mathbf{g}_{\mathbf{k}} \cdot \boldsymbol{\sigma}$ with $\mathbf{g}_{\mathbf{k}} = -\mathbf{g}_{-\mathbf{k}}$ and the Pauli matrices $\boldsymbol{\sigma}$ acting on the spin space [45]. The parity-odd couplings κ_{\pm} , allowed by the parity-broken nature of the noncentrosymmetric superconductors, are nonvanishing but have parametrically small values [15]. Throughout the paper, we use the units $\hbar = c = 1$.

The last term in the gauge derivative \mathcal{D} that appear in the free energy (1) corresponds to the Lifshitz invariant associated with the O point-group symmetry. This term reflects the breaking of the parity symmetry in the system. Indeed, under the parity inversion, $P(\mathbf{x}) = -\mathbf{x}$, the magnetic field transforms as a parity-even quantity $P(\mathbf{B}) = \mathbf{B}$ while the other terms in the derivative transform as vectors, $P(\mathcal{D}_{\pm}) = -\mathcal{D}_{\pm} + 2ie\kappa_{\pm}\mathbf{B}$. Thus, the presence of the last term in the derivative makes the free energy density (1) noninvariant under the parity inversion: $P(\mathcal{F}) = \mathcal{F} - 2ek(\kappa_+ + \kappa_-)\mathbf{B} \cdot \text{Im}(\psi^* \mathcal{D}\psi)$.

The physical length scales of the theory, namely, the coherence length ξ and the London penetration depth λ_L , are determined by the coefficients of the Ginzburg-Landau model as

$$\lambda_L = \lambda_0 \sqrt{1 + \frac{\kappa_+^2 + \kappa_-^2}{2\lambda_0^2}}, \quad \text{where } \lambda_0^2 = \frac{1}{8\pi k e^2 \psi_0^2}, \quad (2a)$$

$$\xi^2 = \frac{k}{2\beta \psi_0^2}, \quad (2b)$$

respectively. Note that in noncentrosymmetric superconductors, an externally applied magnetic field does not decay in a simple monotonic way; for a detailed discussion

of how a counterpart of the London's penetration length is defined in such a case see, *e.g.*, Refs. [19, 20].

The variation of the free energy (1) with respect to the field ψ^* yields the Ginzburg-Landau equation for the superconducting condensate

$$k \sum_{a=\pm} \mathcal{D}_a \mathcal{D}_a \psi = 2\beta(|\psi^2| - \psi_0^2)\psi, \quad (3)$$

while the variation with respect to the vector potential \mathbf{A} determines the Ampère-Maxwell equation

$$\nabla \times \left(\frac{\mathbf{B}}{4\pi} + ke \sum_{a=\pm} \varkappa_a \mathbf{J}_a \right) = ke \sum_{a=\pm} \mathbf{J}_a, \quad (4)$$

where $\mathbf{J}_a = \text{Im}(\psi^* \mathcal{D}_a \psi)$.

The structure of the magnetic field lines can be conveniently characterized by the magnetic helicity:

$$\mathcal{H} = \int \mathbf{A} \cdot \mathbf{B}. \quad (5)$$

It can indeed serve as a measure of the entanglement of the magnetic field lines in knotted configurations of the magnetic field [46]. The magnetic helicity is widely used in ordinary electrically conducting plasmas described by ideal magnetohydrodynamics, where it is a conserved quantity modulo energy-costly reconnections of the magnetic field lines [27].

B. London-limit

The kinetic term of the free energy (1), can be expanded into a sum of gauge-invariant terms:

$$\frac{1}{2} \sum_{a=\pm} |\mathcal{D}_a \psi|^2 = |\mathbf{D}\psi|^2 + \chi \mathbf{j} \cdot \mathbf{B} + e^2(\chi^2 + \nu^2)|\psi|^2 \mathbf{B}^2,$$

$$\text{where } \mathbf{D} := \nabla - ie\mathbf{A} \text{ and } \mathbf{j} = 2e|\psi|^2(\nabla\varphi - e\mathbf{A}). \quad (6)$$

In the London limit the superconducting density is a spatially uniform quantity, $|\psi| = \psi_0$, and the free energy reads as follows [47]:

$$\mathcal{F}_L = k\lambda_L^2 e^2 \psi_0^2 \{ \mathbf{B}^2 + \hat{\mathbf{j}}^2 + 2\Gamma \hat{\mathbf{j}} \cdot \mathbf{B} \}, \quad (7)$$

$$\text{where } \hat{\mathbf{j}} = \frac{\mathbf{j}}{2\lambda_L e^2 \psi_0^2}, \quad \Gamma = \frac{\chi}{\lambda_L}, \quad \text{and } 0 \leq \Gamma \leq 1.$$

Importantly, the dimensionless parameter Γ quantifies the importance of the parity breaking. At $\Gamma = 0$, the material is thus centrosymmetric. The second London equation that relates the magnetic field \mathbf{B} and the current (6) $\mathbf{j} = 2e\psi_0^2(\nabla\varphi - e\mathbf{A})$ takes the following form:

$$\mathbf{B} = \Phi_0 \mathbf{v} - \tilde{\nabla} \times \hat{\mathbf{j}}. \quad (8)$$

Here $\mathbf{v} = \frac{1}{2\pi} \nabla \times \nabla \varphi$ is the density of vortex field that accounts for the phase singularities, and $\Phi_0 = 2\pi/e$ is the superconducting flux quantum. In the dimensionless

units used here $\tilde{\mathbf{x}} = \mathbf{x}/\lambda_L$ and $\tilde{\nabla} = \lambda_L \nabla$, the Ampère-Maxwell equation (4) reads as

$$\tilde{\nabla} \times \mathbf{H} = \tilde{\nabla} \times (\mathbf{B} - 4\pi \mathbf{M}) = \tilde{\mathbf{J}}, \quad (9)$$

$$\text{where } \mathbf{H} = \mathbf{B} + \Gamma \hat{\mathbf{j}}, \quad \tilde{\mathbf{J}} = \hat{\mathbf{j}} + \Gamma \mathbf{B}, \quad \text{and } \mathbf{M} = -\frac{\Gamma \hat{\mathbf{j}}}{4\pi},$$

are, respectively, the (dimensionless) magnetic field, the total current, and the magnetization.

Introducing the complex quantity $\eta = \Gamma + i\sqrt{1-\Gamma^2}$, the free-energy density (7) in the London limit can further be rewritten as

$$\tilde{\mathcal{F}}_L := \frac{\mathcal{F}_L}{k\lambda_L^2 e^2 \psi_0^2} = (\mathbf{B} + \eta \hat{\mathbf{j}})(\mathbf{B} + \eta^* \hat{\mathbf{j}}). \quad (10)$$

The constant density approximation, together with the expression for the magnetic field (8), thus yields the dimensionless free energy:

$$\tilde{\mathcal{F}}_L = (\mathcal{L}^* \hat{\mathbf{j}} - \Phi_0 \mathbf{v}) \cdot (\mathcal{L} \hat{\mathbf{j}} - \Phi_0 \mathbf{v}). \quad (11)$$

Here, for shorthand notation, we introduce the operator $\mathcal{L} \hat{\mathbf{j}} = \tilde{\nabla} \times \hat{\mathbf{j}} - \eta \hat{\mathbf{j}}$. The London equation for the current $\hat{\mathbf{j}}$, obtained as the Euler-Lagrange equation by varying the free energy (11) with respect to $\hat{\mathbf{j}}$, reads as

$$\mathcal{L} \mathcal{L}^* \hat{\mathbf{j}} = \Phi_0 \text{Re}[\mathcal{L}^* \mathbf{v}]. \quad (12)$$

Note that, the source field \mathbf{v} is not a regular function but a distribution that is zero almost everywhere, except for a set of phase singularities identified with positions of vortices. Since we are interested in vortex-free configurations, the source term associated with the vortex fields is, from now on, set to zero $\mathbf{v} = 0$.

As we demonstrate below, the London equation (12) can be seen as a complex, force-free equation whose solution corresponds to the eigenfunctions of the curl operator with complex eigenvalues. The general axisymmetric eigenfunctions of the curl operator can, for example, be found by using the Chandrasekhar-Kendall toroidal-poloidal decomposition [24, 48]. Below, we will express the solutions differently, using the basis of vector spherical harmonics.

III. LOCALIZED FORCE-FREE SOLUTIONS

We are interested in finding the spatially localized solutions of the London equation (12). This equation can be simplified by introducing a complex, force-free vector field \mathcal{Q} that satisfies the force-free equation:

$$\mathcal{L} \mathcal{Q} = 0. \quad (13)$$

Hence, in the absence of a source term, the London equation implies that

$$\mathcal{L}^* \hat{\mathbf{j}} = i \text{Im}(\eta) \mathcal{Q}, \quad (14)$$

where \mathcal{Q} obeys the force-free equation (13). The definition (14) relates the physical magnetic fields and the electric current to the force-free field \mathcal{Q} as

$$\hat{\mathbf{j}} = \text{Re}\mathcal{Q}, \quad \mathbf{J} = \sqrt{1 - \Gamma^2} \text{Im}(\eta\mathcal{Q}), \quad (15a)$$

$$\mathbf{B} = -\text{Re}(\eta\mathcal{Q}), \quad \mathbf{H} = \sqrt{1 - \Gamma^2} \text{Im}(\mathcal{Q}). \quad (15b)$$

It is convenient to represent the solutions \mathcal{Q} of the force-free equation (13) in the basis of the vector spherical harmonics $\mathbf{Z}_{lm} = (\mathbf{Y}_{lm}, \mathbf{\Psi}_{lm}, \mathbf{\Phi}_{lm})$:

$$\mathcal{Q}(\mathbf{x}) = \sum_{l=0}^{\infty} \sum_{m=-l}^{+l} \left(\sum_{\mathbf{Z}=\mathbf{Y},\mathbf{\Psi},\mathbf{\Phi}} Q_{lm}^{\mathbf{Z}}(r) \mathbf{Z}_{lm}(\hat{\mathbf{r}}) \right), \quad (16)$$

where the harmonics \mathbf{Z}_{lm} and the corresponding radial functions $Q_{lm}^{\mathbf{Z}}(r)$ are labeled by the integer-valued quantum number of the angular momentum $l = 0, 1, 2, \dots$ and its projection on the z axis, $m \equiv m_z \in \mathbb{Z}$ with $-l \leq m \leq l$. The angular coordinates are encoded in the unit vector $\hat{\mathbf{r}} \equiv \mathbf{r}/r$. The vector spherical harmonics are defined, in the parametrization of Ref. [49], via their scalar counterpart $Y_{lm}(\hat{\mathbf{r}})$ as

$$\mathbf{Y}_{lm}(\hat{\mathbf{r}}) = Y_{lm}(\hat{\mathbf{r}})\hat{\mathbf{r}}, \quad (17a)$$

$$\mathbf{\Psi}_{lm}(\hat{\mathbf{r}}) = r \nabla Y_{lm}(\hat{\mathbf{r}}), \quad (17b)$$

$$\mathbf{\Phi}_{lm}(\hat{\mathbf{r}}) = \mathbf{r} \times \nabla Y_{lm}(\hat{\mathbf{r}}). \quad (17c)$$

Given the decomposition (16), the force-free equation (13) yields a set of differential equations whose solutions that are bounded at infinity are as follows (see details in Appendix A):

$$Q_{lm}^{\mathbf{\Phi}} = c_{lm} h_l^{(1)}(\eta r), \quad Q_{lm}^{\mathbf{Y}} = -c_{lm} \frac{l(l+1)}{\eta r} h_l^{(1)}(\eta r),$$

$$Q_{lm}^{\mathbf{\Psi}} = -c_{lm} \left(\frac{l+1}{\eta r} h_l^{(1)}(\eta r) - h_{l+1}^{(1)}(\eta r) \right). \quad (18)$$

Here c_{lm} is an arbitrary complex constant, and $h_l^{(1)}(z)$ is the spherical Hankel function of the first kind. Using the relations between the physical fields and the force-free field (15), the total London free energy (11) can be written in the basis of the vector spherical harmonics as

$$\tilde{F} = (1 - \Gamma^2) \sum_{l=0}^{\infty} \sum_{m=-l}^l \int_0^{\infty} r^2 dr \sum_{\mathbf{Z}=\mathbf{Y},\mathbf{\Psi},\mathbf{\Phi}} w_{lm}^{\mathbf{Z}} |Q_{lm}^{\mathbf{Z}}|^2, \quad (19)$$

where $w_{lm}^{\mathbf{Y}} = 1$ and $w_{lm}^{\mathbf{\Phi}} = w_{lm}^{\mathbf{\Psi}} = l(l+1)$. Here, the angular degrees of freedom have been integrated out using the orthogonality properties of the spherical harmonics (see Appendix D). Note that the dimensionless energy (19) is related to the total free energy as $F = k\lambda_L^5 e^2 \psi_0^2 \tilde{F}$.

According to the definitions of the free energy (7), in the absence of phase gradients, the gauge field \mathbf{A} is related to the dimensionless current $\hat{\mathbf{j}}$ as $\mathbf{A} = -\lambda_L \hat{\mathbf{j}}$. Thus, the dimensionless helicity (5) reads as $\tilde{\mathcal{H}} \equiv \mathcal{H}/\lambda_L = -\int \hat{\mathbf{j}} \cdot \mathbf{B}$. Here again, given the relations (15) between

the physical fields and the force-free field \mathcal{Q} , the dimensionless helicity takes the following form:

$$\mathcal{H} = \int \text{Re}(\mathcal{Q}) \cdot \text{Re}(\eta\mathcal{Q}) = \sum_{l,m} \int r^2 dr \mathcal{H}_{lm}, \quad (20)$$

$$\text{where } \mathcal{H}_{lm} = \sum_{\mathbf{Z}=\mathbf{Y},\mathbf{\Psi},\mathbf{\Phi}} w_{lm}^{\mathbf{Z}} \begin{cases} \text{Re}(\eta Q_{lm}^{\mathbf{Z}}) \text{Re}(Q_{lm}^{\mathbf{Z}}) & \text{if } m \text{ even,} \\ \text{Im}(\eta Q_{lm}^{\mathbf{Z}}) \text{Im}(Q_{lm}^{\mathbf{Z}}) & \text{if } m \text{ odd.} \end{cases}$$

At small radius r , all the components of the force-free field (18) are divergent:

$$Q_{lm}^{\mathbf{\Phi}} \sim r^{-(l+2)}, \quad Q_{lm}^{\mathbf{Y}} \sim r^{-(l+2)}, \quad Q_{lm}^{\mathbf{\Psi}} \sim r^{-(l+1)}. \quad (21)$$

Therefore, all the toroflux modes, in the London limit, have an intrinsic divergence at the origin. For example, the divergence of the $l = 1$ solution behaves as a point-like magnetic dipole which, in realistic circumstances, can be regularized by the size of a ferromagnetic (spherical) inclusion that represents a physical dipole. The same statement can also be applied to the other, quadrupole ($l = 2$) and higher modes.

The conventional vortices, in the London limit, are known to have a similar divergence, which is resolved by introducing a cut-off at a short distance from the vortex center. Introducing such a cut-off is relevant because vortices have a nonzero phase winding, and consequently, the complex field of the condensate must vanish somewhere. However, these arguments cannot be applied to the case of the toroflux for the simple reason that the source term associated with the vortex fields is set to zero, $\mathbf{v} = 0$ [see the discussion after Eq. (12)]. Therefore, no topological arguments *demand* vanishing the superconducting density, leading to a breakdown of the London limit that further requires the introduction of an ultraviolet cut-off.

Below we consider a general case of a magnetized inclusion which naturally regularizes the divergence of the toroflux modes (21).

IV. MAGNETIZED INCLUSION

In order to account for the divergences of the force-free field, it is instructive to consider the case of a magnetized (spherical) inclusion in the bulk of the noncentrosymmetric material. The Maxwell equations that determine the magnetic field inside the inclusion are

$$\tilde{\nabla} \times \mathbf{H} = 0, \quad \tilde{\nabla} \cdot \mathbf{B} = 0, \quad \text{where } \mathbf{B} = \mathbf{H} + 4\pi \mathbf{M}. \quad (22)$$

The magnetic field \mathbf{B} and the magnetization \mathbf{M} are decomposed onto the vector spherical harmonics, similarly to the force-free field \mathcal{Q} (16). The fields of the magnetized spherical inclusion are constructed following the standard textbook calculations (see, *e.g.*, [50], for a detailed derivation, see Appendix B). The general solutions are constrained by the requirement that the magnetic field should be a real-valued quantity, while the magnetic

fields $\check{\mathbf{B}}$ and $\check{\mathbf{H}}$ inside the magnetized spherical inclusion of radius r_0 satisfy the following relations:

$$\check{H}_{lm}^{\mathbf{Y}} = \check{H}_{lm}^{\mathbf{\Psi}} = -\frac{4\pi l \check{M}_{lm}^{\mathbf{Y}}}{2l+1} \left(\frac{r}{r_0}\right)^{l-1}, \quad \check{H}_{lm}^{\mathbf{\Phi}} = 0, \quad (23a)$$

$$\check{B}_{lm}^{\mathbf{Z}} = \check{H}_{lm}^{\mathbf{Z}} + 4\pi \check{M}_{lm}^{\mathbf{Z}}, \quad \text{with } \mathbf{Z} = \mathbf{Y}, \mathbf{\Psi}, \mathbf{\Phi}. \quad (23b)$$

The continuity conditions for the current and the magnetic fields at the interface between a magnetized inclusion inside a superconducting medium read as:

$$0 = \mathbf{J} \cdot \mathbf{n}_{12} \Big|_{r=r_0}, \quad (24a)$$

$$0 = \mathbf{n}_{12} \cdot (\mathbf{B}_2 - \mathbf{B}_1) \Big|_{r=r_0}, \quad (24b)$$

$$\mathbf{J}_S = \mathbf{n}_{12} \times (\mathbf{H}_2 - \mathbf{H}_1) \Big|_{r=r_0}. \quad (24c)$$

Here, \mathbf{n}_{12} is the normal vector from medium 1 (the magnetized inclusion) to medium 2 (the parity-breaking superconductor) and \mathbf{J}_S is the surface current density that is localized at the interface. The first equation in Eqs. (24) represents the requirement of the absence of a flow of \mathbf{J} through the interface between the superconductor and the magnetized inclusion [39]. Using the representation (16) of the solution in the basis of the vector spherical harmonics, and given that \mathbf{Y}_{lm} is the only vector harmonic that has a radial component, we represent the first two equations in Eqs. (24) as

$$\mathbf{J} \cdot \mathbf{n}_{12} \Big|_{r=r_0} = \sqrt{1-\Gamma^2} \sum_{l,m} \text{Im}(\eta Q_{lm}^{\mathbf{Y}} Y_{lm}) = 0, \quad (25a)$$

$$(\mathbf{B} - \check{\mathbf{B}}) \Big|_{r=r_0} = -\sum_{l,m} \text{Re}[(\eta Q_{lm}^{\mathbf{Y}} + \check{B}_{lm}^{\mathbf{Y}}) Y_{lm}] = 0. \quad (25b)$$

Note that the intrinsic degrees of freedom of the solutions of these equations always allow one to reconstruct the real-valued magnetic field (23) inside the inclusion. In other words, it is always possible to find the field $\check{\mathbf{B}}$ such that $\text{Im}\check{\mathbf{B}} = 0$. Hence, the interface conditions (25), for a given (l, m) mode, boil down to

$$\eta Q_{lm}^{\mathbf{Y}} + \check{B}_{lm}^{\mathbf{Y}} \Big|_{r=r_0} = 0. \quad (26)$$

Finally, the use of the explicit form of the solutions for the radial functions (18) and the expressions for the fields inside the spherical inclusion (23), provides us with the

matching conditions that fixes the coefficients c_{lm} as

$$c_{lm} = \frac{4\pi r_0 \check{M}_{lm}^{\mathbf{Y}}(r_0)}{l(2l+1)h_l^{(1)}(\eta r_0)} \quad \text{for } l > 0. \quad (27)$$

V. TOROFLUX INDUCED BY A DIPOLE

Consider now the particular case of a spherical impurity of the radius r_0 , with the magnetic dipole moment $\check{\mathbf{M}}$ directed along the axis $\hat{\mathbf{z}}$. In spherical coordinates, the magnetic moment of the impurity reads as follows:

$$\begin{aligned} \check{\mathbf{M}} &= M_0 \hat{\mathbf{z}} = M_0 (\hat{\mathbf{r}} \cos \theta - \hat{\boldsymbol{\theta}} \sin \theta) \\ &= \sqrt{\frac{4\pi}{3}} M_0 (\mathbf{Y}_{10} + \mathbf{\Psi}_{10}). \end{aligned} \quad (28)$$

The continuity conditions (27) fix the only nonzero coefficient c_{10} of the force-free field \mathcal{Q} (16):

$$c_{10} = \frac{r_0 M_0}{h_1^{(1)}(\eta r_0)} \left(\frac{4\pi}{3}\right)^{3/2}. \quad (29)$$

The behavior of the Hankel functions for small arguments implies that

$$c_{10} = i\sqrt{\frac{4\pi}{3}} \left(\frac{4\pi r_0^3}{3}\right) M_0 \eta^2, \quad \text{when } r_0 \rightarrow 0. \quad (30)$$

Thus, for a point-like dipole with the magnetic moment

$$M_0^d = \frac{4\pi}{3} r_0^3 M_0, \quad (31)$$

the coefficient is uniquely determined as

$$c_{10} = i\sqrt{\frac{4\pi}{3}} \eta^2 M_0^d. \quad (32)$$

The quantity M_0 is the density of the magnetic moment in the impurity calculated per unit volume. The related force-free field \mathcal{Q} corresponds to the $(l, m) = (1, 0)$ harmonics:

$$\begin{aligned} \mathcal{Q}_{10} &= -M_0^d \frac{e^{i\eta r}}{\eta r^3} \left[(1 - i\eta r)(2 \cos \theta \hat{\mathbf{r}} + \eta r \sin \theta \hat{\boldsymbol{\phi}}) \right. \\ &\quad \left. + (1 - i\eta r(1 - i\eta r)) \sin \theta \hat{\boldsymbol{\theta}} \right], \end{aligned} \quad (33)$$

where we used the explicit form of spherical Hankel functions of the first kind (18) in order to express the solution in the closed form. An alternative derivation via the Chandrasekhar-Kendall method is briefly outlined in Appendix C. The physical fields can be reconstructed from the force-free field (33) by using the relations (15)

$$\begin{aligned} \mathbf{H} = M_0^d e^{-r\sqrt{1-\Gamma^2}} & \left\{ \frac{2 \cos \theta}{r^3} \left[\left(\sqrt{1-\Gamma^2} + r \right) \cos \Gamma r - \Gamma \sin \Gamma r \right] \hat{\mathbf{r}} \right. \\ & + \frac{\sin \theta}{r^3} \left[\left((1+r^2)\sqrt{1-\Gamma^2} + r \right) \cos \Gamma r + \Gamma(r^2-1) \sin \Gamma r \right] \hat{\boldsymbol{\theta}} \\ & \left. + \frac{\sin \theta}{r^2} \left[\Gamma r \cos \Gamma r - \left(1 + r\sqrt{1-\Gamma^2} \right) \sin \Gamma r \right] \hat{\boldsymbol{\phi}} \right\}, \end{aligned} \quad (34a)$$

$$\begin{aligned} \mathbf{J} = M_0^d e^{-r\sqrt{1-\Gamma^2}} & \left\{ \frac{2 \cos \theta}{r^3} \left[\Gamma r \cos \Gamma r - \left(1 + r\sqrt{1-\Gamma^2} \right) \sin \Gamma r \right] \hat{\mathbf{r}} \right. \\ & + \frac{\sin \theta}{r^3} \left[\Gamma r \left(1 + 2r\sqrt{1-\Gamma^2} \right) \cos \Gamma r - \left(1 + r\sqrt{1-\Gamma^2} + r^2(1-2\Gamma^2) \right) \sin \Gamma r \right] \hat{\boldsymbol{\theta}} \\ & \left. - \frac{\sin \theta}{r^2} \left[\Gamma \left(1 + 2r\sqrt{1-\Gamma^2} \right) \sin \Gamma r + \left(r(1-2\Gamma^2) + \sqrt{1-\Gamma^2} \right) \cos \Gamma r \right] \hat{\boldsymbol{\phi}} \right\}. \end{aligned} \quad (34b)$$

The complex parameter η depends on the parity-breaking parameter $0 \leq \Gamma \leq 1$ as $\eta = \Gamma + i\sqrt{1-\Gamma^2}$. Thus all the fields are exponentially localized at large distances as $e^{-r\sqrt{1-\Gamma^2}}$. Hence, the size of the toroflux,

$$L_{\text{tor}} = \frac{\lambda_L}{\sqrt{1-\Gamma^2}}, \quad (35)$$

is determined by the London penetration length λ_L and the dimensionless parity-breaking coupling Γ defined in Eq. (7). In the limit of the maximal parity violation, $\Gamma \rightarrow 1$, the size of the toroflux diverges.

The present construction of the toroflux solutions, induced by a magnetized source in a noncentrosymmetric superconductor, is done in the London limit approximation, where the amplitude of the superconducting condensate is fixed. This implies that only the magnetic energy and kinetic energy of supercurrents are taken into account and thus assumes that there is no suppression of the order parameter. In the textbook case of conventional vortices, the London approximation breaks down near the vortex core, where the kinetic and magnetic energy densities are large enough to suppress the superconducting condensate. A similar situation should also be realized for the toroflux, and thus the kinetic energy density of supercurrents could not grow indefinitely. Instead, when the sum of the kinetic and magnetic energy densities becomes comparable to condensation energy density, the modulus of the order parameter should get suppressed $|\psi(\mathbf{r})| < \psi_0$. This results in the formation of a core like structure where the growth of kinetic energy is limited by the depletion of the density of the order parameter.

It is instructive to estimate when the London approximation breaks down. To this end, we compare the energy densities \mathcal{F} , Eqs. (1), of two possible configurations. First is \mathcal{F}_1 , the energy density of the toroflux in the London approximation where $\psi = \psi_0$, while the second is \mathcal{F}_2 , the energy of a normal state ($\psi = 0$), with the same magnetic field configuration. Hence the London approximation can be expected to break where $\mathcal{F}_1 > \mathcal{F}_2$. The

energy \mathcal{F}_2 is thus

$$\mathcal{F}_2 = \frac{\mathbf{B}^2}{8\pi} + \frac{\beta\psi_0^4}{2} = \frac{(M_0^d)^2[5+3\cos(2\theta)]}{16\pi r^6} + \frac{\beta\psi_0^4}{2}, \quad (36)$$

where the magnetic field \mathbf{B} is that of the toroflux solution given by (33) inserted into (15). The energy \mathcal{F}_1 , in the London approximation, is obtained from (7) [again by inserting (33) into (15)]:

$$\mathcal{F}_1 = \frac{(M_0^d)^2[5+3\cos(2\theta)]}{16\pi r^6} \left(1 + \frac{\nu^2}{\lambda_0^2} \right). \quad (37)$$

The requirement that $\mathcal{F}_1 > \mathcal{F}_2$ can then be cast into the following inequality:

$$r^6 < \frac{(M_0^d)^2 \nu^2 [5+3\cos(2\theta)]}{8\pi\beta\psi_0^4 \lambda_0^2}. \quad (38)$$

Now, we want to ensure that our London approximation works reasonably everywhere outside the magnetic inclusion. Hence the cutoff r_c , which corresponds to the maximal possible radius r of the impurity where the London theory breaks down, is obtained from Eq. (38) with $\theta = 0$:

$$r_c = (4\epsilon M_0^d \nu \xi)^{1/3}. \quad (39)$$

It is interesting to note that the cutoff scale in the case of a toroflux is not simply $\propto \xi$ as for usual vortices, but is $\propto \xi^3$ with a dependence on the size and magnetization of the impurity. Then our approximation will work everywhere if $r_c < r_0$, which results in the following condition, expressed via the parameters of the model (2):

$$\frac{16\pi}{3} \nu \xi \epsilon M_0 < 1, \quad (40)$$

or, equivalently,

$$\frac{32\pi^2 M_0 \xi \sqrt{\lambda_L^2 (1-\Gamma^2) - \lambda_0^2}}{3\Phi_0} < 1. \quad (41)$$

Note that this condition can always be satisfied for sufficiently small magnetic moment M_0 .

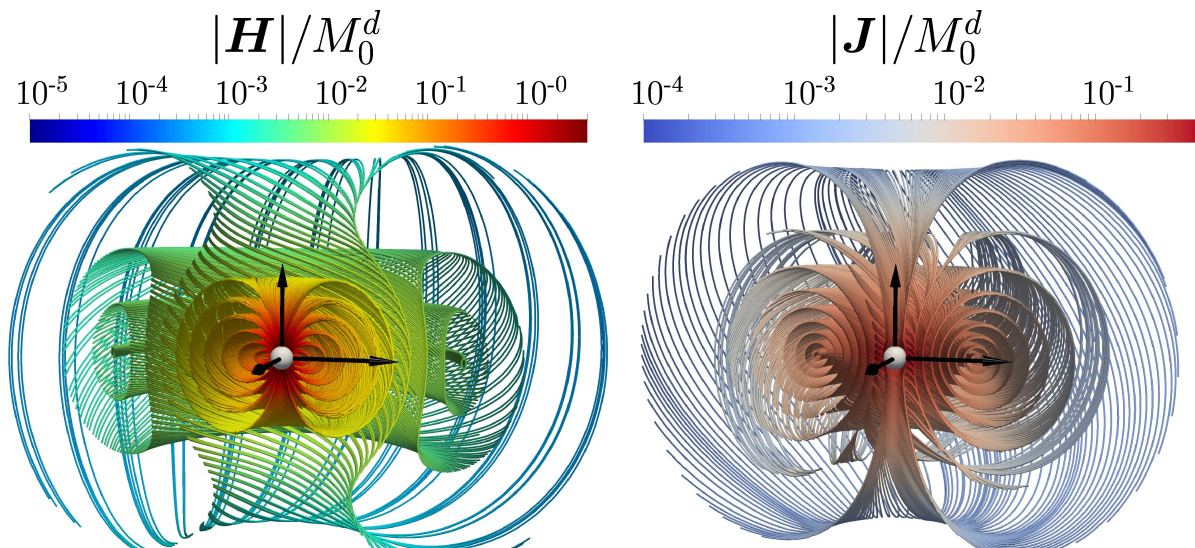


Figure 1. A toroflux solution induced by a magnetic dipole for the parity-breaking parameter $\Gamma = 0.5$. The left panel displays the streamlines of the magnetic field \mathbf{H} , while the right panel shows the streamlines of the total electric current \mathbf{J} . These quantities are related to each other via the Ampère-Maxwell equation (9). The sphere in the center shows the position of the magnetized inclusion (the magnetic dipole).

A. Knotted nature of the toroflux

The physical fields \mathbf{H} and \mathbf{J} (34) associated with the force-free field \mathcal{Q}_{10} induced by a magnetic dipole (33) are displayed in Fig. 1, for the value of the parity-breaking parameter $\Gamma = 0.5$. This figure illustrates that a magnetic dipole impurity induces, in a noncentrosymmetric superconductor, the knotted lines of both the magnetic field and the electric current. These toroidal, axially symmetric, nested structures resemble in many aspects the standard Chandrasekhar-Kendall states [24]. The alternative derivation of our solutions, presented in Appendix C, highlights the proximity of the toroflux and the Chandrasekhar-Kendall states. Note that since the magnetic lines of the toroflux are closed, the total flux through any cross section of the solution vanishes identically.

The London penetration depth determines the overall length scale of the toroflux without affecting the geometry of its internal structure. On the contrary, the strength of the noncentrosymmetry strongly affects the overall structure of the toroflux. The latter feature is illustrated in Fig. 2, which shows the streamlines of the magnetic field \mathbf{H} and the electric current \mathbf{J} as well as their Poincaré sections of the torofluxes for moderate ($\Gamma = 0.15$), intermediate ($\Gamma = 0.5$), and high ($\Gamma = 0.95$) values of the parity-breaking parameter Γ .

At small parity breaking ($\Gamma = 0.15$), the magnetic field lines resemble that of a magnetic dipole. They are attached to the magnetized inclusion and slightly twisted around the axis of the dipole (and the chirality of twist depends on the sign of Γ). Accordingly, the current flows around the dipole and covers various tori. When the noncentrosymmetry becomes more impor-

tant ($\Gamma = 0.5$), the toroflux features nested tori of the magnetic lines, in addition to the twisted structure near the dipole. This property can be seen, in particular, in the $\mathbf{H}|_{x=0}$ Poincaré section in Fig. 2. Interestingly, the chirality of the extra nested tori is reversed compared to the set of field lines that are attached to the dipole. Upon increase of the parity breaking, additional sets of nested tori appear, as can be seen in the $\mathbf{H}|_{x=0}$ Poincaré section in Fig. 2 for $\Gamma = 0.95$. The fact that the number of tori with opposite chirality increases as the parity breaking becomes stronger is qualitatively similar to the effect of the magnetic field inversion observed near vortices at large Γ reported in Refs. [19, 20].

B. Energy and helicity of the toroflux

The dimensionless energy (19) of the toroflux solution (33) induced by a magnetic dipole depends on the parity-breaking parameter Γ as

$$\tilde{F}(\Gamma, r_0) = \frac{2(M_0^d)^2}{r_0^3} e^{-2r_0\sqrt{1-\Gamma^2}} \left[(1 + 2r_0^2)(1 - \Gamma^2) + [2(1 - \Gamma^2) + r_0^2] r_0 \sqrt{1 - \Gamma^2} \right]. \quad (42)$$

The exponential prefactor contains the ratio of the inclusion radius r_0 with the size (35) of the toroflux, which is the consequence of the Meissner effect.

Figure 3 shows the toroflux energy (42) as a function of the parity-breaking parameter Γ . The toroflux energy monotonically decreases as the parity breaking parameter Γ , and it is maximal in the centrosymmetric limit, $\Gamma \rightarrow 0$. This property is a consequence of the Lifshitz

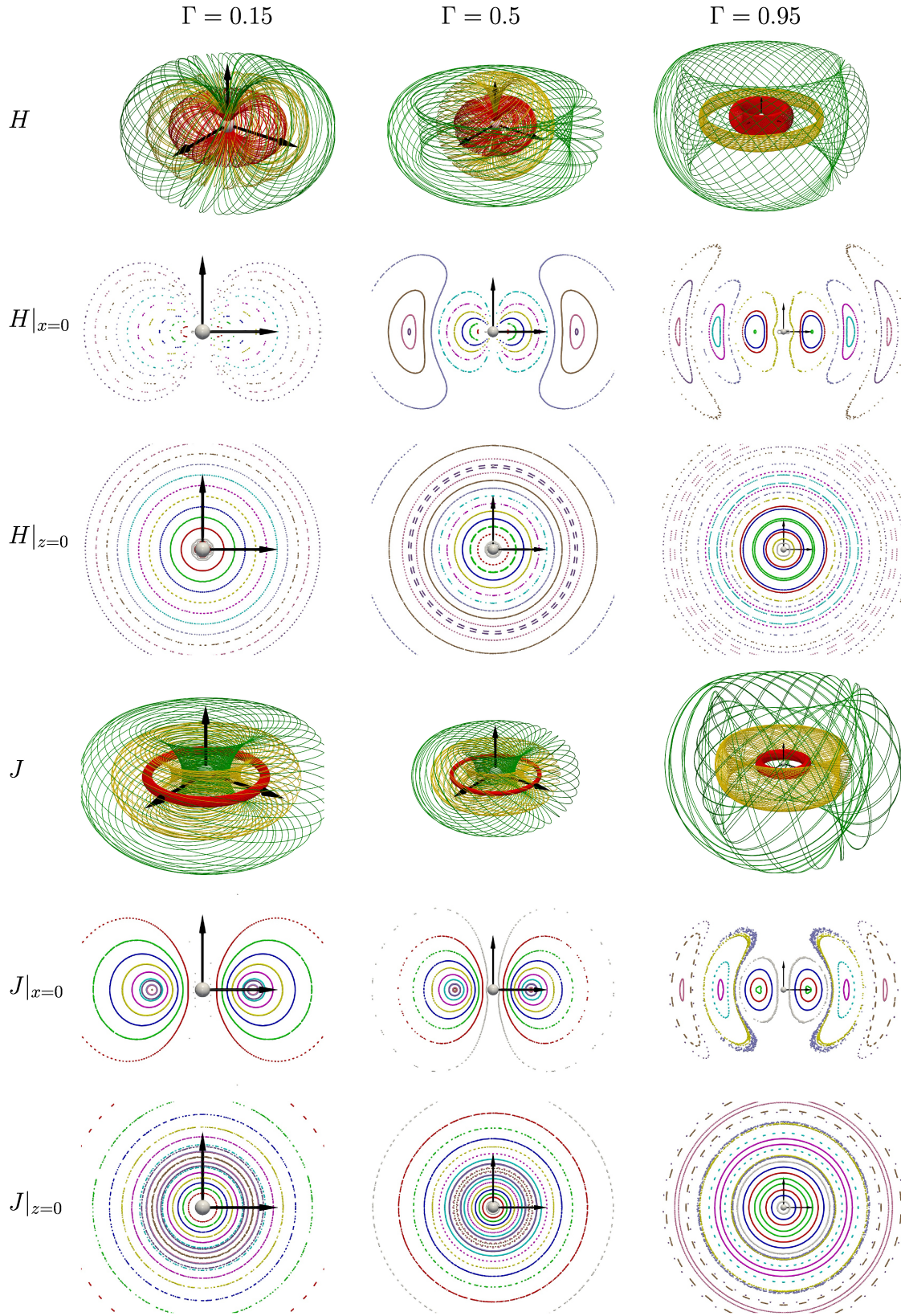


Figure 2. The structure of the streamlines of the magnetic field \mathbf{H} and the electric current \mathbf{J} , of the toroflux solution induced by a magnetic dipole, for the values of the parity-breaking parameter $\Gamma = 0.15, 0.5$, and 0.95 . The line on the top row shows the streamlines of \mathbf{H} , and the two next rows are the Poincaré sections of the streamlines of \mathbf{H} on the $x = 0$ and $z = 0$ planes, respectively. Similarly, the block of the three bottom rows indicates the structure of the current \mathbf{J} . The central sphere depicts the spherical magnetic dipole inclusion. The relative sizes of the torofluxes can be seen from the vector basis.

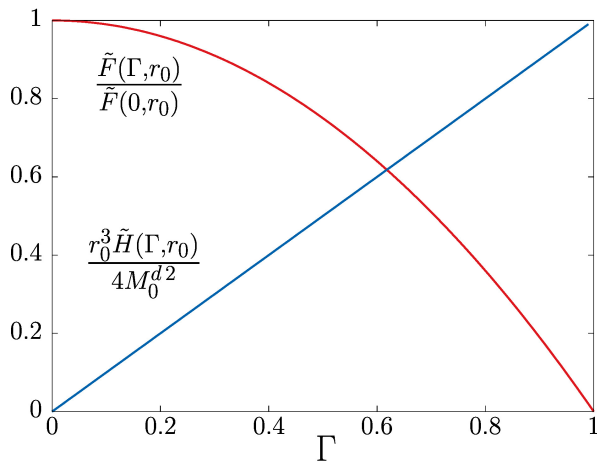


Figure 3. The normalized free energy \tilde{F} and the normalized helicity \tilde{H} of the toroflux as functions of the parity breaking coupling Γ for the spherical magnetic dipole impurity of the radius $r_0 = 10^{-2}$ (in units of λ_L).

term $\mathbf{j} \cdot \mathbf{B}$, which provides a negative contribution when the electric current and the magnetic field are (partially) aligned. When Γ reaches the upper bound, $\Gamma = 1$, the toroflux energy vanishes while its size (35) diverges. Note that unlike vortices, which carry a quantized magnetic flux, the toroflux has a zero net flux through any plane that intersects the magnetic dipole impurity. The amplitude of the magnetic field is determined only by the magnetization of the dipole, hence the energy of our toroflux solution is not quantized.

Figure 3 also displays the helicity (20) of the toroflux, which, unlike the energy, monotonically grows with the increase of the parity-breaking parameter Γ . As the non-linear corrections are small for small (with respect to the London penetration depth) inclusions $r_0 \ll 1$, the helicity is almost a linear function of Γ . The leading contribution to the helicity at the small radius r_0 reads explicitly as follows:

$$\begin{aligned} \frac{\mathcal{H}(\Gamma, r_0)}{2(M_0^d)^2} &= \frac{2\Gamma[1 + r_0^2(\Gamma^2 + 1)]}{r_0^3} - 2(\Gamma^5 + 4\Gamma^3 - 3\Gamma) \\ &+ \frac{8\Gamma^5 + 12\Gamma^3 - 17\Gamma}{3\sqrt{1 - \Gamma^2}} + O(r_0^2). \end{aligned} \quad (43)$$

As previously stated, the magnetic helicity, which is associated with the topological properties of the magnetic field lines, serves as the measure of the linking of knotted lines of the magnetic field \mathbf{B} . In this respect, it is worth mentioning that the helicity of magnetic fields (5) cannot be associated with an ordinary topological charge because this quantity is not quantized in terms of integer numbers. However, magnetic helicity is a topological quantity as it has a topological origin: a measure of the degree of linking of magnetic field lines. The non-quantization appears as a result of the standard definition (5), which scales quadratically with the magnitude of magnetic field ($\mathcal{H} \rightarrow \alpha^2 \mathcal{H}$ if the gauge field is scaled by

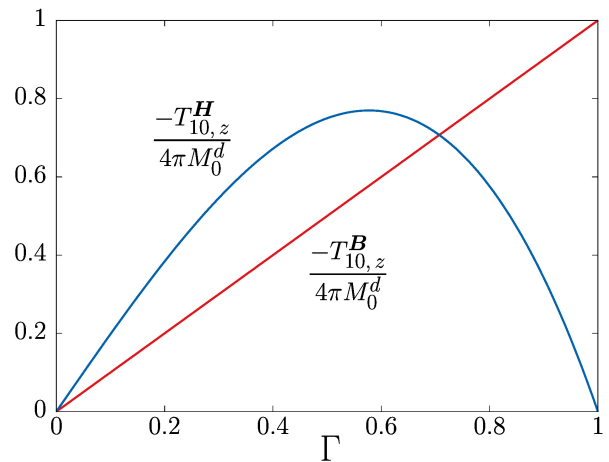


Figure 4. The amplitude of the toroidal dipole moments of the toroflux induced by a pointlike magnetic dipole, as functions of the parity-breaking coupling Γ . The toroidal dipole moment associated with the induction \mathbf{T}_{10}^B grows linearly with Γ , taking its maximum at the maximal value of the parity-breaking parameter, $\Gamma = 1$. Quite surprisingly, unlike \mathbf{T}_{10}^B , the magnetic dipole moment \mathbf{T}_{10}^H is maximal at $\Gamma = 1/\sqrt{3}$, and vanishes at maximal parity breaking.

a factor of α as $\mathbf{A} \rightarrow \alpha \mathbf{A}$). The helicity is a very useful characteristic of the magnetic field in force-free environments, represented, for example, by ideal magnetohydrodynamics in perfectly conducting plasmas (e.g., in the solar corona) [27, 46], which are ungapped counterparts of noncentrosymmetric superconductors.

Notice that the limit of a vanishing magnetic helicity, $\Gamma \rightarrow 0$, smoothly connects the toroflux ($\Gamma \neq 0$) with a topologically trivial screened magnetic dipole solution ($\Gamma = 0$). Despite the energy of the solution does not vanish and does not become singular, the toroflux solution disappears because, at $\Gamma = 0$, the magnetic helicity of the configuration expectedly vanishes, and the toroflux solution becomes the usual dipole field screened by the superconducting condensate.

C. Toroidal dipole moments

Beyond the magnetic helicity, the toroflux solutions can be characterized by additional global quantities: the toroidal dipole moments. The multipole expansions are central to various areas of physics [51, 52]. In particular, the *toroidal dipole moments* have been demonstrated to play an important role in the electrodynamics of various condensed matter systems (for reviews, see [52–54]). The toroidal dipole moments of the magnetic field \mathbf{H} and the induction \mathbf{B} are respectively defined as

$$\mathbf{T}^H = \frac{1}{2} \int \mathbf{r} \times \mathbf{H}, \quad \text{and} \quad \mathbf{T}^B = \frac{1}{2} \int \mathbf{r} \times \mathbf{B}. \quad (44)$$

Given the relation (15) between the physical fields and the force-free field \mathcal{Q}_{10} (33) induced by a point-like

dipole, the toroidal dipole moments (44) of the associated toroflux are (see Appendix B 3 for detailed derivation)

$$\mathbf{T}_{10}^{\mathbf{H}} = -8\pi M_0^d \Gamma (1 - \Gamma^2) \hat{z} \quad \text{and} \quad \mathbf{T}_{10}^{\mathbf{B}} = -4\pi M_0^d \Gamma \hat{z}. \quad (45)$$

It follows, as illustrated in Fig. 4, that both toroidal dipole moments vanish in the centrosymmetric case. Interestingly, unlike $\mathbf{T}_{10}^{\mathbf{B}}$, which is a linear function of the parity-breaking parameter Γ , the toroidal moment $\mathbf{T}_{10}^{\mathbf{H}}$ also vanishes at maximal parity breaking $\Gamma = 1$. The observation of a toroidal dipole moment of either \mathbf{B} or \mathbf{H} thus unambiguously signals the presence of a toroflux induced by a magnetic dipole.

D. Probing toroflux with muon spins

The toroflux states could, in principle, be detected with the muon-spin spectroscopy [55]. This method is a powerful tool to probe magnetic fields inside superconductors, allowing one to shed light on their superconducting properties [56, 57].

The muon-spin spectroscopy involves implanting spin-polarized positively charged muons (also called antimuons) in the bulk of the sample. After coming to rest inside the material, the spin of each muon starts to precess about the axis of the local magnetic field. The precession, however, does not last long, as the muon decays with a half-life of 2.2 μs . The crucial ingredient of the method is that the product of the decay, a positron, carries information about the direction of the muon spin at the time of the decay. Therefore, the measurement of the spatial distribution of the emitted positrons probes the local magnetic environment inside the materials. In addition, the method is susceptible to weak field variations, which makes it especially useful in probing the internal field structure.

The decomposition of the positron spectrum over the vector spherical harmonic modes yields direct information on the knottedness of the toroflux lines, which, in turn, can provide information about the parity-breaking parameter Γ . In our paper, we do not discuss the details of the experimental techniques. Instead, we assume that the spectrum gives information about the spherical modes of the magnetic field, in a natural extension of the earlier experiments [56, 57].

Since the experiment detects the volume-averaged flux of positrons, the positron spectrum is insensitive to the position of the toroflux inside the sample but is susceptible to the toroflux orientation. Setting the coordinate system along the axial symmetry vector of the toroflux, the magnetic moments of the magnetic field \mathbf{H} of the toroflux solution are

$$a_{lm,l'm'}^{\mathbf{Z}} = \int d^3r \mathbf{H}_{lm}(\mathbf{r}) \mathbf{Z}_{l'm'}(\mathbf{r}). \quad (46)$$

For the simplest $(l, m) = (1, 0)$ solution, given explicitly in Eq. (34), the monopole component is obviously

zero, $a_{00}^{\mathbf{Z}} = 0$ (where for short we note $a_{l'm'}^{\mathbf{Z}} \equiv a_{10,l'm'}^{\mathbf{Z}}$). For the experimentally relevant small values of the radius $r_0 \ll 1$, the $(l', m') = (1, 0)$ dipole-moment components take the following form:

$$\begin{aligned} a_{10}^{\mathbf{Y}} &= -4M_0^d \sqrt{\frac{\pi}{3}} \left[(\ln r_0 + \gamma_E - 1) \cos \Gamma + \Gamma \sin \Gamma \right] + O(r_0^2), \\ a_{10}^{\mathbf{\Psi}} &= 4M_0^d \sqrt{\frac{\pi}{3}} \left[(\ln r_0 + \gamma_E - 2) \cos \Gamma + \Gamma \sin \Gamma \right] + O(r_0^2), \\ a_{10}^{\mathbf{\Phi}} &= 8M_0^d \sqrt{\frac{\pi}{3}} \sin \Gamma + O(r_0), \end{aligned} \quad (47)$$

where γ_E is the Euler-Mascheroni constant. In the centrosymmetric limit $\Gamma \rightarrow 0$, the radial, $a_{10}^{\mathbf{Y}}$, and polar, $a_{10}^{\mathbf{\Psi}}$, dipole components of the toroflux solution are nonvanishing. These components are characteristics of an ordinary magnetic dipole that possesses a trivial, unknotted magnetic field [58]. However, the presence of a nonvanishing azimuthal dipole component, $a_{10}^{\mathbf{\Phi}} \propto \Gamma$, which could potentially be detected in a muon-spin spectroscopy, can be considered as a clear sign of the presence of the knotted magnetic lines that are inherent to our toroflux solution.

The nonvanishing $a_{10}^{\mathbf{\Phi}}$ component (47) is calculated in the (laboratory) coordinate system in which the z axis is coaligned with the magnetic dipole moment of the impurity. If these axes are misaligned, then, in a general coordinate system, the toroflux-sensitive coefficient $a_{10}^{\mathbf{\Phi}}$ will be different from the result of Eq. (47). The difference between the system associated with the toroflux and the laboratory coordinate system is given by a spatial rotation with a matrix \hat{R} . Under rotation, the (l, m) vector spherical harmonics transformed linearly into each other with the proportionality coefficients given by the Wigner D matrices [59]. In particular, $\hat{R} \Phi_{lm} = \sum_{m'=-l}^l D_{mm'}^l \Phi_{lm'}$. Substituting this equation into the definition of the magnetic moments (46), we observe by an explicit calculation that for the $(l, m) = (1, 0)$ toroflux solution (34), the component $a_{10}^{\mathbf{\Phi}}$ is nonzero (47), while the other two components with $m = \pm 1$ vanish, $a_{1,\pm 1}^{\mathbf{\Phi}} \equiv 0$. Therefore, in the rotated coordinate system, the Φ magnetic dipole moment is given by $a_{10}^{\mathbf{\Phi}}(\vartheta) = D_{00}^1(\vartheta) a_{10}^{\mathbf{\Phi}}$, where $a_{10}^{\mathbf{\Phi}}$ is the magnetic moment in the local system associated with the toroflux solution and ϑ is the angle between the symmetry axis of the toroflux and the z axis of the laboratory system.

Taking into account the value of the corresponding Wigner matrix, $D_{00}^1 = \cos \vartheta$, one gets

$$a_{10}^{\mathbf{\Phi}}[\vartheta] = 4M_0^d \sqrt{\frac{\pi}{3}} \Gamma \cos \vartheta. \quad (48)$$

The Φ component of the magnetic moment (48) has the same properties as the usual magnetic moment because it measures the projection of the dipole moment onto the z axis. Its value is maximal when the z axis is coaligned with the axis of the toroflux ($\vartheta = 0$), and it vanishes when the axes are perpendicular to each other ($\vartheta = \pi/2$). Detecting a nonvanishing coefficient $a_{10}^{\mathbf{\Phi}}$, for example, in a

muon-spin experiment, should signal the presence of the toroflux induced by a magnetic dipole. Since the importance of the κ_{\pm} term in the Ginzburg-Landau functional strongly depends on the temperature [20], it will also help differentiate the effects of noncentrosymmetry from the effects caused by a random polarization of magnetic inclusions.

VI. CONCLUSION

We demonstrated that noncentrosymmetric superconductors with broken inversion symmetry host a family of stable configurations with self-knotted magnetic field lines. These states, which we call *toroflux*, are superconducting counterparts of the Chandrasekhar-Kendall states that play an important role in highly conducting, force-free plasmas relevant to astrophysical research and applications in nuclear fusion [24, 25]. The Meissner effect forces the spatial localization of the toroflux solutions, thus making them different from the conventional Chandrasekhar-Kendall states.

Working in the London limit, we demonstrate that the size of the toroflux is determined by the London penetration length λ_L and the dimensionless parity breaking parameter $0 \leq \Gamma \leq 1$, as $L_{\text{tor}} = \lambda_L / \sqrt{1 - \Gamma^2}$. In the limit of the maximal parity violation, $\Gamma \rightarrow 1$, the size of the toroflux diverges.

The knotted nature of the toroflux states is rooted in the parity-breaking magnetoelectric effect that generates the supercurrent along the magnetic field lines. The supercurrent also produces the magnetic field, thus linking the magnetic field lines of the toroflux. The toroflux is characterized by a non-vanishing toroidal dipole moment of the magnetic field that linearly depends on the parity-breaking parameter Γ . They are also characterized by the helicity of the magnetic field, which vanishes in the absence of the parity breaking ($\Gamma = 0$). In this limit, the knottedness disappears, and the configuration of magnetic fields reduces to an ordinary dipole screened by the superconducting condensate. Since the toroflux is characterized by a nonvanishing magnetic helicity, in the $\Gamma \rightarrow 0$ limit, the toroflux solution disappears. Thus, the broken parity (with $\Gamma \neq 0$) in a noncentrosymmetric superconductor plays a crucial role in the existence of the toroflux since no such configurations are possible in an ordinary superconductor with unbroken parity.

The torofluxes constitute an infinitely high tower of solutions labeled by orbital $0 \leq l < \infty$ and magnetic $-l \leq m \leq l$ quantum numbers. Although the energy of any (l, m) -toroflux diverges at its core in the London limit, one could argue that toroflux energy should be finite beyond this limit (similarly to the energy density of conventional vortices, which is divergent in the London limit if a core cutoff is neglected and finite otherwise). In our paper, we focus on the toroflux solutions sourced by a weak magnetic inclusion. The size of the inclusion serves as a short-distance cutoff that regularizes the solu-

tion and makes the toroflux energy finite. Going beyond the London limit, for small inclusion and solutions with large energy density, a natural cutoff will be provided by density suppression (a corelike structure), with a minimal size given by the coherence length. Detailed investigation of this question, however, goes beyond the scope of the current work.

We show that a finite-sized ferromagnetic inclusion with an (l, m) -multipole moment regularizes the divergences and thus induces an (l, m) toroflux with finite energy. The most physically relevant case we discussed here in detail is the case of a magnetic dipole inclusion $(l, m) = (1, 0)$. Note that in all generality, our solutions are regularized by any finite-size magnetized inclusion with a nonvanishing (l, m) -multipole moment.

Our findings could open up the possibility to extract new information about noncentrosymmetric superconductors from muon-spin rotation probes. We have demonstrated that the distribution of magnetic field polarization of toroflux solutions is principally different from a dipole field configuration of a magnetic impurity in a conventional superconductor. It could potentially allow us to extract the parameters \varkappa_{\pm} from the statistics of the polarization of magnetic field sensed by muons.

ACKNOWLEDGMENTS

We thank Vadim Grinenko for the discussions. A. K. and A. M. were supported by Grant No. 0657-2020-0015 of the Ministry of Science and Higher Education of Russia. A. M. is grateful for the kind hospitality extended to him by the Theory Group during his stay at the Institut Denis Poisson (Tours, France), where this work was completed. A. S. and E. B. were supported by the Swedish Research Council Grants No. 2016-06122, No. 2018-03659, and No. 2022-04763.

Appendix A: Detailed derivation of a general solution via vector spherical harmonics

We derive a general solution of the force-free equation $\mathcal{L}\mathcal{Q} = 0$ using the basis of the spherical vector harmonics [49], which provides a convenient separation of the radial and angular variables. The force-free field \mathcal{Q} , as well as the other fields, are thus decomposed as follows:

$$\mathcal{Q}(\mathbf{x}) = \sum_{l=0}^{\infty} \sum_{m=-l}^{+l} \left(\sum_{\mathbf{Z}=\mathbf{Y}, \mathbf{\Psi}, \mathbf{\Phi}} Q_{lm}^{\mathbf{Z}}(r) \mathbf{Z}_{lm}(\hat{\mathbf{r}}) \right). \quad (\text{A1})$$

Here $\mathbf{Z}_{lm} = (\mathbf{Y}_{lm}, \mathbf{\Psi}_{lm}, \mathbf{\Phi}_{lm})$ are the three orthogonal vector spherical harmonics, defined as [49]

$$\mathbf{Y}_{lm}(\hat{\mathbf{r}}) = Y_{lm}(\hat{\mathbf{r}})\hat{\mathbf{r}}, \quad (\text{A2a})$$

$$\mathbf{\Psi}_{lm}(\hat{\mathbf{r}}) = r \nabla Y_{lm}(\hat{\mathbf{r}}), \quad (\text{A2b})$$

$$\mathbf{\Phi}_{lm}(\hat{\mathbf{r}}) = \mathbf{r} \times \nabla Y_{lm}(\hat{\mathbf{r}}), \quad (\text{A2c})$$

where $Y_{lm}(\hat{\mathbf{r}})$ are the scalar spherical harmonics which depend on the angular coordinates encoded in the unit vector $\hat{\mathbf{r}} \equiv \mathbf{r}/r$. See Appendix D for details on the definitions and properties of the vector spherical harmonics.

Given the decomposition (A1), the force-free vector equation $\mathcal{L}\mathcal{Q} = 0$ determines a system of three differential equations:

$$-\frac{l(l+1)}{\eta r} Q_{lm}^{\Phi} - \eta Q_{lm}^{\mathbf{Y}} = 0, \quad (\text{A3a})$$

$$-\frac{1}{r} \frac{d}{dr} (r Q_{lm}^{\Phi}) - \eta Q_{lm}^{\Psi} = 0, \quad (\text{A3b})$$

$$\frac{1}{r} \frac{d}{dr} (r Q_{lm}^{\Psi}) - \frac{1}{r} Q_{lm}^{\mathbf{Y}} - \eta Q_{lm}^{\Phi} = 0, \quad (\text{A3c})$$

which, combined together, yields

$$Q_{lm}^{\mathbf{Y}} = -\frac{l(l+1)}{\eta r} Q_{lm}^{\Phi}, \quad Q_{lm}^{\Psi} = -\frac{1}{\eta r} \frac{d}{dr} (r Q_{lm}^{\Phi}), \quad (\text{A4a})$$

$$\left[\frac{1}{r^2} \frac{d}{dr} \left(r^2 \frac{d}{dr} \right) - \frac{l(l+1)}{r^2} + \eta^2 \right] Q_{lm}^{\Phi} = 0. \quad (\text{A4b})$$

Equation (A4b) on Q_{lm}^{Φ} is the spherical Bessel equation whose general solution is the superposition of two spherical Hankel functions

$$Q_{lm}^{\Phi} = c_{lm} h_l^{(1)}(\eta r) + d_{lm} h_l^{(2)}(\eta r). \quad (\text{A5})$$

Here, $h_l^{(1)}$ and $h_l^{(2)}$ are, respectively, the Hankel functions of the first and second kind.

1. Hankel functions

The spherical Hankel functions are expressed via the spherical Bessel functions as [60]

$$h_l^{(1)}(z) = j_l(z) + iy_l(z), \quad h_l^{(2)}(z) = j_l(z) - iy_l(z), \quad (\text{A6})$$

where, in turn, the spherical Bessel functions are related to the Bessel functions of half-integer order:

$$j_l(z) = \sqrt{\frac{2\pi}{z}} J_{l+1/2}(z), \quad y_l(z) = \sqrt{\frac{2\pi}{z}} Y_{l+1/2}(z), \quad (\text{A7})$$

with J_l and Y_l being respectively the Bessel functions of the first and second kind. Note that for a non-negative rank l , the spherical Hankel function of the first kind can be expressed in a closed form,

$$h_l^{(1)}(z) = (-i)^{l+1} \frac{e^{iz}}{z} \sum_{p=0}^l (-i2z)^{-p} \frac{(l+p)!}{p!(l-p)!}, \quad (\text{A8})$$

and the Hankel function of the second kind can be obtained in a similar way using the definition in Eq. (A6).

2. Asymptotics

For large $|z|$, when $-\pi < \arg z < \pi$, the spherical Hankel functions have the following asymptotic behavior at the large argument [60]:

$$h_l^{(1)}(z) \sim \frac{2\pi}{z} \exp \left[i \left(z - \frac{(l+1)\pi}{2} \right) \right], \quad (\text{A9a})$$

$$h_l^{(2)}(z) \sim \frac{2\pi}{z} \exp \left[-i \left(z - \frac{(l+1)\pi}{2} \right) \right]. \quad (\text{A9b})$$

By definition, $\eta = \Gamma + i\sqrt{1-\Gamma^2}$ with $\Gamma \in [0, 1]$, so that $0 < \arg(\eta r) < \pi$ and thus

$$h_l^{(1)}(\eta r) \sim \frac{2\pi(-i)^{l+1}}{\eta r} e^{+i\Gamma r} e^{-\sqrt{1-\Gamma^2}r}, \quad (\text{A10a})$$

$$h_l^{(2)}(\eta r) \sim \frac{2\pi(i)^{l+1}}{\eta r} e^{-i\Gamma r} e^{+\sqrt{1-\Gamma^2}r}. \quad (\text{A10b})$$

Hence, the second spherical Hankel functions diverges at large r . It follows that for the solutions (A5) to be bounded at infinity, we must have $d_{lm} = 0$, and thus

$$Q_{lm}^{\Phi} = c_{lm} h_l^{(1)}(\eta r). \quad (\text{A11})$$

Finally, given the defining relations (A4a), the asymptotically finite components of the force-free field, associated with the different vector spherical harmonics are

$$Q_{lm}^{\Phi} = c_{lm} h_l^{(1)}(\eta r), \quad Q_{lm}^{\mathbf{Y}} = -c_{lm} \frac{l(l+1)}{\eta r} h_l^{(1)}(\eta r),$$

$$Q_{lm}^{\Psi} = -c_{lm} \left(\frac{l+1}{\eta r} h_l^{(1)}(\eta r) - h_{l+1}^{(1)}(\eta r) \right), \quad (\text{A12})$$

where c_{lm} is an arbitrary complex constant.

3. Behaviour at small r

At small z , the spherical Hankel function behaves as [60]

$$h_l^{(1)}(z) = \frac{-i2^l \Gamma(l+1/2)}{\sqrt{\pi} z^{l+1}}. \quad (\text{A13})$$

It follows that the leading contributions of the different components of the force-free field at small r are

$$Q_{lm}^{\mathbf{Y}} = c_{lm} \frac{i2^l l(l+1)\Gamma(l+1/2)}{\sqrt{\pi} \eta^{l+2} r^{l+2}}, \quad (\text{A14a})$$

$$Q_{lm}^{\Psi} = c_{lm} \frac{i2^l l \Gamma(l+1/2)}{\sqrt{\pi} \eta^{l+2} r^{l+2}}, \quad (\text{A14b})$$

$$Q_{lm}^{\Phi} = -c_{lm} \frac{i2^l \Gamma(l+1/2)}{\sqrt{\pi} \eta^{l+1} r^{l+1}}. \quad (\text{A14c})$$

Thus, at small radius r , all the components of the force-free field diverge as

$$Q_{lm}^{\Phi} \sim r^{-(l+2)}, \quad Q_{lm}^{\mathbf{Y}} \sim r^{-(l+2)}, \quad Q_{lm}^{\Psi} \sim r^{-(l+1)}. \quad (\text{A15})$$

It follows that all of the toroflux modes have an intrinsic divergence at the origin, and therefore they require a regularization, or a cutoff, at the core of the solutions. We demonstrate in the next Appendix that such a regularization can consistently be done.

Appendix B: Magnetized spherical inclusion

Here, we consider the case of a magnetized inclusion in the bulk of the noncentrosymmetric medium. For simplicity, we study a spherical inclusion of radius r_0 , as it is schematically illustrated in Fig. 5. Inside a magnetized medium, the constituent magnetostatics equations are

$$\tilde{\nabla} \times \mathbf{H} = 0, \quad \tilde{\nabla} \cdot \mathbf{B} = 0 \quad \text{where} \quad \mathbf{B} = \mathbf{H} + 4\pi \mathbf{M}. \quad (\text{B1})$$

The fields of the magnetized spherical inclusion are constructed following the standard textbook calculations (see, *e.g.*, [50]). To this end, we introduce the magnetic scalar potential ω_M , which describes the magnetic field $\mathbf{H} = -\tilde{\nabla}\omega_M$, and decompose the magnetic potential over the (scalar) spherical harmonics. It follows that

$$\mathbf{H} = -\sum_{l=0}^{\infty} \sum_{m=-l}^{+l} \frac{d\omega_{lm}}{dr} \mathbf{Y}_{lm} + \frac{\omega_{lm}}{r} \boldsymbol{\Psi}_{lm}, \quad (\text{B2a})$$

$$\text{where} \quad \left[\frac{d^2}{dr^2} + 2r \frac{d}{dr} - l(l+1) \right] \omega_{lm} = 0, \quad (\text{B2b})$$

where the second equation follows from the relation $\tilde{\nabla} \cdot \mathbf{H} = 0$ which reflects the closeness of the lines of the field \mathbf{H} . This determines the magnetic potential associated with the magnetized inclusion:

$$\omega_{lm} = \begin{cases} \check{c}_{lm} r^l & \text{if } r < r_0 \\ \check{d}_{lm} r^{-(l+1)} & \text{if } r > r_0. \end{cases} \quad (\text{B3})$$

Hereafter, the symbol $\check{\cdot}$ marks the quantities inside the spherical inclusion.

The continuity of the magnetic potential at the boundary $r = r_0$ implies that $\check{d}_{lm} = \check{c}_{lm} r_0^{2l+1}$. The normal derivative of the magnetic potential is discontinuous across the interface. Therefore, the relation $\nabla \cdot (\mathbf{H} + 4\pi \mathbf{M}) = 0$ implies that, at $r = r_0$,

$$\frac{d\omega_{lm}^{\text{in}}}{dr} - \frac{d\omega_{lm}^{\text{out}}}{dr} = 4\pi \check{M}_{lm}^{\mathbf{Y}} \Rightarrow \check{c}_{lm} = \frac{4\pi \check{M}_{lm}^{\mathbf{Y}}}{(2l+1)r_0^{l-1}}. \quad (\text{B4})$$

Here, $\check{M}_{lm}^{\mathbf{Y}}$ is the \mathbf{Y} component of the magnetization $\check{\mathbf{M}}$, decomposed over the vector spherical harmonics analogously to (16). Hence, the magnetic fields inside the magnetized spherical inclusion are

$$\check{H}_{lm}^{\mathbf{Y}} = \check{H}_{lm}^{\boldsymbol{\Psi}} = -\frac{4\pi l \check{M}_{lm}^{\mathbf{Y}}}{2l+1} \left(\frac{r}{r_0} \right)^{l-1}, \quad \check{H}_{lm}^{\boldsymbol{\Phi}} = 0, \quad (\text{B5a})$$

$$\check{B}_{lm}^{\mathbf{Z}} = \check{H}_{lm}^{\mathbf{Z}} + 4\pi \check{M}_{lm}^{\mathbf{Z}}, \quad \text{with } \mathbf{Z} = \mathbf{Y}, \boldsymbol{\Psi}, \boldsymbol{\Phi}. \quad (\text{B5b})$$

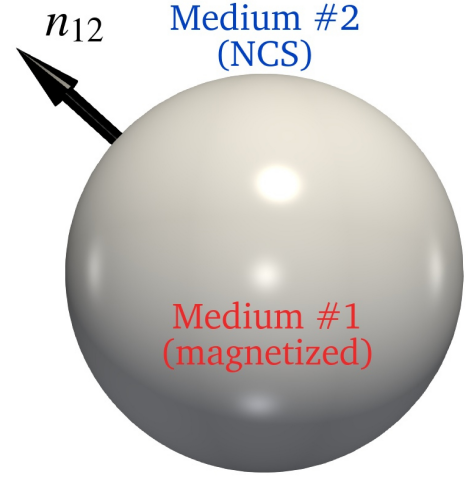


Figure 5. Schematic representation of a spherical magnetized medium (#1) of radius r_0 and the noncentrosymmetric superconducting medium (#2). The unit vector \mathbf{n}_{12} is the normal vector at the interface between these media.

As detailed below, the interface boundary conditions between the magnetized inclusion and the superconductor allow one to relate the values of the parameters c_{lm} between both media.

1. Matching conditions at the interface

The continuity conditions for the current and the magnetic fields at the interface between a magnetized inclusion inside a superconducting medium read as:

$$0 = \mathbf{J} \cdot \mathbf{n}_{12} \Big|_{r=r_0}, \quad (\text{B6a})$$

$$0 = \mathbf{n}_{12} \cdot (\mathbf{B}_2 - \mathbf{B}_1) \Big|_{r=r_0}, \quad (\text{B6b})$$

$$\mathbf{J}_S = \mathbf{n}_{12} \times (\mathbf{H}_2 - \mathbf{H}_1) \Big|_{r=r_0}. \quad (\text{B6c})$$

Here, \mathbf{n}_{12} is the normal vector from medium 1 (the magnetized inclusion) to the medium 2 (the parity-odd superconductor) and \mathbf{J}_S is the surface current density that is localized at the interface, Fig. 5.

The first equation in Eqs. (B6) states that the superconducting current \mathbf{J} does not enter the non-superconducting magnetized inclusion [39]. Consequently, the normal component of \mathbf{J} vanishes at the interface between these media. Given the decomposition (A1) over the vector spherical harmonics, and since \mathbf{Y}_{lm} is the only vector harmonic that has a radial component, the first two relations in Eqs. (B6) reduce to

$$\mathbf{J} \cdot \mathbf{n}_{12} \Big|_{r=r_0} = \sqrt{1 - \Gamma^2} \sum_{l,m} \text{Im}(\eta Q_{lm}^{\mathbf{Y}} Y_{lm}) = 0, \quad (\text{B7a})$$

$$(\mathbf{B} - \check{\mathbf{B}}) \Big|_{r=r_0} = -\sum_{l,m} \text{Re}[(\eta Q_{lm}^{\mathbf{Y}} + \check{B}_{lm}^{\mathbf{Y}}) Y_{lm}] = 0. \quad (\text{B7b})$$

Note that there is always the freedom to construct the magnetic field $\tilde{\mathbf{B}}$ inside the spherical inclusion, so that it is real. It is thus always possible to construct $\tilde{\mathbf{B}}$ such that $\text{Im}\tilde{\mathbf{B}} = 0$. Hence, the conditions (B7) at the interface, for a given mode (l, m) , boil down to

$$\eta Q_{lm}^{\mathbf{Y}} + \tilde{B}_{lm}^{\mathbf{Y}}|_{r=r_0} = 0. \quad (\text{B8})$$

Finally, we use the explicit form of the radial modes (A12) to fix all the coefficients c_{lm} of the solution:

$$c_{lm} = \frac{r_0 \tilde{B}_{lm}^{\mathbf{Y}}(r_0)}{l(l+1)h_l^{(1)}(\eta r_0)} \quad \text{for } l > 0. \quad (\text{B9})$$

Now, given the (l, m) magnetization modes of the magnetized spherical inclusion (B5), the arbitrary coefficient c_{lm} reads as

$$c_{lm} = \frac{4\pi r_0 \tilde{M}_{lm}^{\mathbf{Y}}(r_0)}{l(2l+1)h_l^{(1)}(\eta r_0)} \quad \text{for } l > 0. \quad (\text{B10})$$

Thus, we obtain the most general solution for a spherical inclusion with arbitrary magnetization.

2. Ferromagnetic inclusion and magnetic dipole

Consider now the particular case of a spherical inclusion of radius r_0 , which possesses a magnetic dipole moment $\tilde{\mathbf{M}}$ directed along the axis $\hat{\mathbf{z}}$, and with all higher-order modes vanishing. In spherical coordinates, the magnetic moment reads as

$$\begin{aligned} \tilde{\mathbf{M}} &= M_0 \hat{\mathbf{z}} = M_0 (\hat{\mathbf{r}} \cos \theta - \hat{\boldsymbol{\theta}} \sin \theta) \\ &= \sqrt{\frac{4\pi}{3}} M_0 (\mathbf{Y}_{10} + \boldsymbol{\Psi}_{10}). \end{aligned} \quad (\text{B11a})$$

Thus, the magnetic fields (B5) inside the inclusion are

$$\tilde{H}_{10}^{\mathbf{Y}} = \tilde{H}_{10}^{\boldsymbol{\Psi}} = -\left(\frac{4\pi}{3}\right)^{3/2} M_0, \quad \tilde{H}_{10}^{\boldsymbol{\Phi}} = 0, \quad (\text{B12a})$$

$$\tilde{B}_{10}^{\mathbf{Y}} = \tilde{B}_{10}^{\boldsymbol{\Psi}} = 2\left(\frac{4\pi}{3}\right)^{3/2} M_0, \quad \tilde{B}_{10}^{\boldsymbol{\Phi}} = 0. \quad (\text{B12b})$$

Finally, given the continuity conditions, the free coefficient c_{10} (B10) in this case becomes

$$c_{10} = \frac{r_0 M_0}{h_1^{(1)}(\eta r_0)} \left(\frac{4\pi}{3}\right)^{3/2}. \quad (\text{B13})$$

The behavior of the Hankel functions for small arguments (A13), implies that

$$c_{10} = i\sqrt{\frac{4\pi}{3}} \left(\frac{4\pi r_0^3}{3}\right) M_0 \eta^2, \quad \text{when } r_0 \rightarrow 0. \quad (\text{B14})$$

Thus, for a pointlike dipole with the magnetic moment $M_0^d = \frac{4\pi}{3} r_0^3 M_0$, the coefficient is uniquely determined as

$$c_{10} = i\sqrt{\frac{4\pi}{3}} \eta^2 M_0^d. \quad (\text{B15})$$

Now, given the coefficient (B15), the magnetic field \mathbf{H} and the current \mathbf{J} induced by a magnetic pointlike dipole can be reconstructed from the force-free field \mathbf{Q} according to (15). The components of the force-free field \mathbf{Q} corresponding to a given sector of the vector spherical harmonics are defined in terms of the spherical Hankel functions of the first kind (18). These functions can further be expressed in a closed form using the relation (A8). Finally, the vector harmonics of a dipolar source possess the single mode $(l, m) = (1, 0)$, which has the simple form (D12). Thus, in terms of elementary functions, the force-free field \mathbf{Q}_{10} induced by a magnetic dipole reads as

$$\begin{aligned} \mathbf{Q}_{10} &= -M_0^d \frac{e^{i\eta r}}{\eta r^3} \left[(1 - i\eta r)(2 \cos \theta \hat{\mathbf{r}} + \eta r \sin \theta \hat{\boldsymbol{\phi}}) \right. \\ &\quad \left. + [1 - i\eta r(1 - i\eta r)] \sin \theta \hat{\boldsymbol{\theta}} \right]. \end{aligned} \quad (\text{B16})$$

3. Toroidal dipole moments

The multipole expansions are central in many areas of physics [51, 52]. A particularly interesting kind of multipole moments are the *toroidal moments*, which play an important role in the electrodynamics of various condensed matter systems (for reviews, see [52–54]). The toroidal dipole moments of the magnetic field \mathbf{H} and the induction \mathbf{B} are respectively defined as

$$\mathbf{T}^{\mathbf{H}} = \frac{1}{2} \int \mathbf{r} \times \mathbf{H} \quad \text{and} \quad \mathbf{T}^{\mathbf{B}} = \frac{1}{2} \int \mathbf{r} \times \mathbf{B}. \quad (\text{B17})$$

Given the relation between the physical fields (15) and the force-free field \mathbf{Q}_{10} (B16) induced by a pointlike dipole, the toroidal dipole moments (45) of the associated toroflux thus read as

$$\mathbf{T}_{10}^{\mathbf{H}} = -\frac{1}{2} \text{Re} \left[\eta \sum_{\mathbf{Z}=\mathbf{Y}, \boldsymbol{\Psi}, \boldsymbol{\Phi}} \int Q_{10}^{\mathbf{Z}} (\mathbf{r} \times \mathbf{Z}_{10}) \right], \quad (\text{B18})$$

$$\mathbf{T}_{10}^{\mathbf{B}} = \frac{\sqrt{1-\Gamma^2}}{2} \text{Im} \left[\sum_{\mathbf{Z}=\mathbf{Y}, \boldsymbol{\Psi}, \boldsymbol{\Phi}} \int Q_{10}^{\mathbf{Z}} (\mathbf{r} \times \mathbf{Z}_{10}) \right].$$

It is thus necessary to evaluate the volume integral

$$\int Q_{10}^{\mathbf{Z}} (\mathbf{r} \times \mathbf{Z}_{10}) = \int r^3 Q_{10}^{\mathbf{Z}} dr \int \hat{\mathbf{r}} \times \mathbf{Z}_{10}(\hat{\mathbf{r}}) d\Omega. \quad (\text{B19})$$

To this end, note the property of the vector spherical harmonics

$$\hat{\mathbf{r}} \times \mathbf{Y}_{lm}(\hat{\mathbf{r}}) = 0, \quad (\text{B20a})$$

$$\hat{\mathbf{r}} \times \boldsymbol{\Psi}_{lm}(\hat{\mathbf{r}}) = \boldsymbol{\Phi}_{lm}(\hat{\mathbf{r}}), \quad (\text{B20b})$$

$$\hat{\mathbf{r}} \times \boldsymbol{\Phi}_{lm}(\hat{\mathbf{r}}) = -\boldsymbol{\Psi}_{lm}(\hat{\mathbf{r}}), \quad (\text{B20c})$$

and that the only non-vanishing integral over the sphere here is $\int \boldsymbol{\Psi}_{10} d\Omega = 2\sqrt{\frac{4\pi}{3}} \hat{\mathbf{z}}$ (see details in Appendix D3). Moreover the radial integral also gives a simple relation

$$\int r^3 h^{(1)}(\eta r) dr = \frac{3i}{\eta^4}. \quad (\text{B21})$$

Thus, given the coefficient c_{10} (B15) associated with the pointlike magnetic dipole, the volume integral (B19) becomes

$$\sum_{\mathbf{Z}=\mathbf{Y}, \boldsymbol{\Psi}, \boldsymbol{\Phi}} \int Q_{10}^{\mathbf{Z}}(\mathbf{r} \times \mathbf{Z}_{10}) = (8\pi M_0^d \eta^{*2}) \hat{\mathbf{z}}. \quad (\text{B22})$$

Finally, using this relation together with the definition of toroidal dipole moments (B18) yields the relations

$$\mathbf{T}_{10}^{\mathbf{H}} = -8\pi M_0^d \Gamma(1 - \Gamma^2) \hat{\mathbf{z}} \quad \text{and} \quad \mathbf{T}_{10}^{\mathbf{B}} = -4\pi M_0^d \Gamma \hat{\mathbf{z}}. \quad (\text{B23})$$

Appendix C: Outline of the Chandrasekhar-Kendall approach for a dipole source

The above section provides the explicit forms of the toroflux solutions induced by a dipole. These can alternatively be derived via the Chandrasekhar-Kendall method [24]. Consider a case when we want to find the magnetic field \mathbf{B} that satisfies the following equation:

$$\mathcal{L}\mathcal{L}^* \mathbf{B} = c \nabla \times (\nabla \times \mathbf{M}^d) + d \nabla \times \mathbf{M}^d, \quad (\text{C1})$$

where c and d are some real parameters and \mathbf{M}^d is a field that corresponds to an external field induced by a magnetic moment. Then, the magnetic field \mathbf{B} can be solved in terms of the following functions:

$$\mathbf{B} = -\text{Re}(\eta \mathcal{Q}), \quad (\text{C2a})$$

$$\mathcal{Q} = \nabla \times \mathbf{u} + \nabla \times (\nabla \times \mathbf{u}) / \eta, \quad (\text{C2b})$$

$$\Delta \mathbf{u} + \eta^2 \mathbf{u} = b \mathbf{M}^d, \quad b = -i(d + c\eta) / \text{Im}\eta. \quad (\text{C2c})$$

where \mathbf{u} is found from solving the inhomogeneous vector Helmholtz equation (C2c). The set of equations (C2) can be verified by showing that

$$\mathcal{L}\mathcal{Q} = -b \nabla \times \mathbf{M}^d / \eta, \quad (\text{C3})$$

which subsequently implies Eq. (C1).

In the simplest case of pointlike dipole source $\mathbf{M}^d = M_0^d \hat{\mathbf{z}} \delta(\mathbf{r})$, the explicit solution of the Helmholtz equation (C2c) is

$$\mathbf{u} = -M_0^d \hat{\mathbf{z}} b \frac{e^{i\eta r}}{4\pi r}. \quad (\text{C4})$$

Note, that values of c and b depend on boundary conditions that are used between magnetized and superconducting mediums. The boundary conditions (B8) are given by

$$(\eta \mathcal{Q} + \check{\mathbf{B}}) \cdot \hat{\mathbf{r}}|_{r=r_0} = 0. \quad (\text{C5})$$

For $\check{\mathbf{B}}(r_0) = 2M_0^d \hat{\mathbf{z}} / r_0^3$ this results in the constants being $c = 4\pi$ and $d = -4\pi \text{Re}\eta$ (and thus $b = 4\pi$).

Now, given the values of c and d that satisfy the appropriate boundary condition, inserting the solution (C4) of the Helmholtz equation into the constituting equation (C2b) yields the very same expression for the force-free field \mathcal{Q} as the explicit form of Eq. (B16).

Appendix D: Spherical harmonics

The scalar spherical harmonics are defined as [60]

$$Y_{lm}(\hat{\mathbf{r}}) = (-1)^m \sqrt{\frac{2l+1}{4\pi} \frac{(l-m)!}{(l+m)!}} P_l^m(\cos\theta) e^{im\phi}, \quad (\text{D1})$$

where P_l^m are the associated Legendre polynomials. The spherical harmonics depend on the polar θ and azimuthal ϕ angles expressed collectively via the unit vector $\hat{\mathbf{r}} \equiv \mathbf{r}/r$. The spherical harmonics satisfy the orthonormality condition:

$$\int d\Omega Y_{lm}(\hat{\mathbf{r}}) Y_{l'm'}^*(\hat{\mathbf{r}}) = \delta_{ll'} \delta_{mm'}, \quad (\text{D2})$$

where $Y_{lm}^* \equiv (-1)^m Y_{l,-m}$ and $d\Omega = \sin\theta d\theta d\phi$ is the solid-angle element.

Adopting the parametrization of Ref. [49], the vector spherical harmonics are defined via their scalar counterpart in Eq. (A2). In a given (l, m) sector, the vector spherical harmonics are locally orthogonal to each other at every point of the unit sphere:

$$\mathbf{Y}_{lm}(\hat{\mathbf{r}}) \cdot \boldsymbol{\Psi}_{lm}(\hat{\mathbf{r}}) = 0, \quad (\text{D3a})$$

$$\mathbf{Y}_{lm}(\hat{\mathbf{r}}) \cdot \boldsymbol{\Phi}_{lm}(\hat{\mathbf{r}}) = 0, \quad (\text{D3b})$$

$$\boldsymbol{\Psi}_{lm}(\hat{\mathbf{r}}) \cdot \boldsymbol{\Phi}_{lm}(\hat{\mathbf{r}}) = 0. \quad (\text{D3c})$$

They also satisfy the normalization and orthogonality relations:

$$\int d\Omega \mathbf{Y}_{lm}(\hat{\mathbf{r}}) \cdot \mathbf{Y}_{l'm'}^*(\hat{\mathbf{r}}) = \delta_{ll'} \delta_{mm'}, \quad (\text{D4a})$$

$$\int d\Omega \boldsymbol{\Phi}_{lm}(\hat{\mathbf{r}}) \cdot \boldsymbol{\Phi}_{l'm'}^*(\hat{\mathbf{r}}) = l(l+1) \delta_{ll'} \delta_{mm'}, \quad (\text{D4b})$$

$$\int d\Omega \boldsymbol{\Psi}_{lm}(\hat{\mathbf{r}}) \cdot \boldsymbol{\Psi}_{l'm'}^*(\hat{\mathbf{r}}) = l(l+1) \delta_{ll'} \delta_{mm'}, \quad (\text{D4c})$$

$$\int d\Omega \mathbf{Y}_{lm}(\hat{\mathbf{r}}) \cdot \boldsymbol{\Psi}_{l'm'}^*(\hat{\mathbf{r}}) = 0, \quad (\text{D4d})$$

$$\int d\Omega \mathbf{Y}_{lm}(\hat{\mathbf{r}}) \cdot \boldsymbol{\Phi}_{l'm'}^*(\hat{\mathbf{r}}) = 0, \quad (\text{D4e})$$

$$\int d\Omega \Phi_{lm}(\hat{\mathbf{r}}) \cdot \Psi_{l'm'}^*(\hat{\mathbf{r}}) = 0, \quad (\text{D4f})$$

where

$$\mathbf{Z}_{lm}^* \equiv (-1)^m \mathbf{Z}_{l,-m}, \quad (\text{D5})$$

for $\mathbf{Z}_{lm} = (\mathbf{Y}_{lm}, \Psi_{lm}, \Phi_{lm})$.

1. Differential operators on vector spherical harmonics

The divergence of the vector spherical harmonics is:

$$\nabla \cdot (f(r) \mathbf{Y}_{lm}) = \left(\frac{df}{dr} + \frac{2}{r} f \right) Y_{lm}, \quad (\text{D6a})$$

$$\nabla \cdot (f(r) \Psi_{lm}) = -\frac{l(l+1)}{r} f Y_{lm}, \quad (\text{D6b})$$

$$\nabla \cdot (f(r) \Phi_{lm}) = 0. \quad (\text{D6c})$$

Similarly, the curl of the vector spherical harmonics gives

$$\nabla \times (f(r) \mathbf{Y}_{lm}) = -\frac{1}{r} f \Phi_{lm}, \quad (\text{D7a})$$

$$\nabla \times (f(r) \Psi_{lm}) = \left(\frac{df}{dr} + \frac{1}{r} f \right) \Phi_{lm} \quad (\text{D7b})$$

$$\nabla \times (f(r) \Phi_{lm}) = -\frac{l(l+1)}{r} f \mathbf{Y}_{lm} - \left(\frac{df}{dr} + \frac{1}{r} f \right) \Psi_{lm}. \quad (\text{D7c})$$

These relations allow one to express the divergence,

$$\nabla \cdot \mathbf{G} = \sum_{l=0}^{\infty} \sum_{m=-l}^l \left(\frac{1}{r^2} \frac{d}{dr} (r^2 G_{lm}^{\mathbf{Y}}) - \frac{l(l+1)}{r} G_{lm}^{\Psi} \right) Y_{lm}, \quad (\text{D8})$$

The basis for $l = 2$ vector spherical functions is as follows:

$$\begin{aligned} \mathbf{Y}_{20} &= \frac{1}{4} \sqrt{\frac{5}{\pi}} (3 \cos^2 \theta - 1) \hat{\mathbf{r}}, & \mathbf{Y}_{21} &= -\sqrt{\frac{15}{8\pi}} e^{i\phi} \sin \theta \cos \theta \hat{\mathbf{r}}, & \mathbf{Y}_{22} &= \frac{1}{4} \sqrt{\frac{15}{2\pi}} e^{2i\phi} \sin^2 \theta \hat{\mathbf{r}}, \\ \Psi_{20} &= -\frac{3}{2} \sqrt{\frac{5}{\pi}} \sin \theta \cos \theta \hat{\boldsymbol{\theta}}, & \Psi_{21} &= -\sqrt{\frac{15}{8\pi}} e^{i\phi} (\cos 2\theta \hat{\boldsymbol{\theta}} + i \cos \theta \hat{\boldsymbol{\phi}}), & \Psi_{22} &= \sqrt{\frac{15}{8\pi}} e^{2i\phi} \sin \theta (\cos \theta \hat{\boldsymbol{\theta}} + i \hat{\boldsymbol{\phi}}), \\ \Phi_{20} &= -\frac{3}{2} \sqrt{\frac{5}{\pi}} \sin \theta \cos \theta \hat{\boldsymbol{\phi}}, & \Phi_{21} &= \sqrt{\frac{15}{8\pi}} e^{i\phi} (i \cos \theta \hat{\boldsymbol{\theta}} - \cos 2\theta \hat{\boldsymbol{\phi}}), & \Phi_{22} &= \sqrt{\frac{15}{8\pi}} e^{2i\phi} \sin \theta (-i \hat{\boldsymbol{\theta}} + \cos \theta \hat{\boldsymbol{\phi}}), \end{aligned} \quad (\text{D13})$$

3. Integrals of spherical functions

The nonvanishing integrals are as follows:

$$\int d\Omega \mathbf{Y}_{10} = \frac{1}{2} \int d\Omega \Psi_{10} = \sqrt{\frac{4\pi}{3}} \hat{\mathbf{z}}, \quad \int d\Omega \mathbf{Y}_{11} = \frac{1}{2} \int d\Omega \Psi_{11} = -\sqrt{\frac{2\pi}{3}} (\hat{\mathbf{x}} + i \hat{\mathbf{y}}). \quad (\text{D14})$$

and the curl,

$$\begin{aligned} \nabla \times \mathbf{G} &= \sum_{l=0}^{\infty} \sum_{m=-l}^l \left[-\frac{l(l+1)}{r} G_{lm}^{\Phi} \mathbf{Y}_{lm} \right. \\ &\quad - \left(\frac{dG_{lm}^{\Phi}}{dr} + \frac{1}{r} G_{lm}^{\Phi} \right) \Psi_{lm} \\ &\quad \left. + \left(-\frac{1}{r} G_{lm}^{\mathbf{Y}} + \frac{dG_{lm}^{\Psi}}{dr} + \frac{1}{r} G_{lm}^{\Psi} \right) \Phi_{lm} \right], \quad (\text{D9}) \end{aligned}$$

of a generic vector:

$$\mathbf{G}(\mathbf{r}) = \sum_{l=0}^{\infty} \sum_{m=-l}^l \left(\sum_{\mathbf{Z}=\mathbf{Y}, \Psi, \Phi} G_l^{\mathbf{Z}}(r) \mathbf{Z}_{lm}(\hat{\mathbf{r}}) \right). \quad (\text{D10})$$

2. First vector spherical harmonics

It is useful to consider a first few spherical harmonics explicitly. Note that the harmonics with negative indices m can be obtained from the equations below, using the conjugacy relation (D5).

The lowest $l = 0$ harmonics is a trivial hedgehog as it possesses a radial component only:

$$\mathbf{Y}_{00} = \frac{1}{\sqrt{4\pi}} \hat{\mathbf{r}}, \quad \Psi_{00} = 0, \quad \Phi_{00} = 0. \quad (\text{D11})$$

The first nontrivial vector spherical harmonics starts from the orbital momentum $l = 1$:

$$\begin{aligned} \mathbf{Y}_{10} &= \sqrt{\frac{3}{4\pi}} \cos \theta \hat{\mathbf{r}}, & \mathbf{Y}_{11} &= -\sqrt{\frac{3}{8\pi}} e^{i\phi} \sin \theta \hat{\mathbf{r}}, \\ \Psi_{10} &= -\sqrt{\frac{3}{4\pi}} \sin \theta \hat{\boldsymbol{\theta}}, & \Psi_{11} &= -\sqrt{\frac{3}{8\pi}} e^{i\phi} (\cos \theta \hat{\boldsymbol{\theta}} + i \hat{\boldsymbol{\phi}}), \\ \Phi_{10} &= -\sqrt{\frac{3}{4\pi}} \sin \theta \hat{\boldsymbol{\phi}}, & \Phi_{11} &= \sqrt{\frac{3}{8\pi}} e^{i\phi} (i \hat{\boldsymbol{\theta}} - \cos \theta \hat{\boldsymbol{\phi}}). \end{aligned}$$

* garaud.phys@gmail.com

† maxim.chernodub@idpoisson.fr

- [1] M. Tinkham, *Introduction To Superconductivity* (McGraw-Hill, 1995) p. 454.
- [2] F. N. Rybakov, J. Garaud, and E. Babaev, Stable Hopf-Skyrme topological excitations in the superconducting state, *Physical Review B* **100**, 094515 (2019).
- [3] See, e.g., <https://en.wikipedia.org/wiki/Toroflux>.
- [4] L. N. Bulaevskii, A. A. Guseinov, and A. I. Rusinov, Superconductivity in crystals without symmetry centers, *Soviet Journal of Experimental and Theoretical Physics* **44**, 1243 (1976), [Russian original: Zh. Eksp. Teor. Fiz. 71, 2356-2372 (1976)].
- [5] L. S. Levitov, Y. V. Nazarov, and G. M. Éliashberg, Magnetostatics of superconductors without an inversion center, *Soviet Journal of Experimental and Theoretical Physics Letters* **41**, 445 (1985), [Russian original: Pis'ma Zh. Eksp. Teor. Fiz. 41, 365 (1985)].
- [6] V. P. Mineev and K. V. Samokhin, Helical phases in superconductors, *Soviet Journal of Experimental and Theoretical Physics* **78**, 401 (1994), [Russian original: Zh. Eksp. Teor. Fiz. 105, 747 (1994)].
- [7] V. M. Edelstein, The Ginzburg - Landau equation for superconductors of polar symmetry, *Journal of Physics: Condensed Matter* **8**, 339 (1996).
- [8] D. F. Agterberg, Novel magnetic field effects in unconventional superconductors, *Physica C: Superconductivity* **387**, 13 (2003), Proceedings of the 3rd Polish-US Workshop on Superconductivity and Magnetism of Advanced Materials.
- [9] K. V. Samokhin, Magnetic properties of superconductors with strong spin-orbit coupling, *Physical Review B* **70**, 104521 (2004).
- [10] E. Bauer, G. Hilscher, H. Michor, C. Paul, E. W. Scheidt, A. Griбанov, Y. Seropegin, H. Noël, M. Sigrist, and P. Rogl, Heavy Fermion Superconductivity and Magnetic Order in Noncentrosymmetric CePt₃Si, *Physical Review Letters* **92**, 027003 (2004).
- [11] K. V. Samokhin, E. S. Zijlstra, and S. K. Bose, CePt₃Si: An unconventional superconductor without inversion center, *Physical Review B* **69**, 094514 (2004).
- [12] H. Q. Yuan, D. F. Agterberg, N. Hayashi, P. Badica, D. Vandervelde, K. Togano, M. Sigrist, and M. B. Salamon, *S*-Wave Spin-Triplet Order in Superconductors without Inversion Symmetry: Li₂Pd₃B and Li₂Pt₃B, *Physical Review Letters* **97**, 017006 (2006).
- [13] A. S. Cameron, Y. S. Yerin, Y. V. Tymoshenko, P. Y. Portnichenko, A. S. Sukhanov, M. C. Hatnean, D. M. K. Paul, G. Balakrishnan, R. Cubitt, A. Heinemann, and D. S. Inosov, Rotation of the magnetic vortex lattice in Ru₇B₃ driven by the effects of broken time-reversal and inversion symmetry, *Physical Review B* **100**, 024518 (2019).
- [14] R. Khasanov, R. Gupta, D. Das, A. Amon, A. Leithe-Jasper, and E. Svanidze, Multiple-gap response of type-I noncentrosymmetric BeAu superconductor, *Physical Review Research* **2**, 023142 (2020).
- [15] E. Bauer and M. Sigrist, *Non-Centrosymmetric Superconductors: Introduction and Overview*, edited by E. Bauer and M. Sigrist, Lecture notes in physics (Springer Berlin Heidelberg, 2012).
- [16] S. Yip, Noncentrosymmetric Superconductors, *Annual Review of Condensed Matter Physics* **5**, 15 (2014).
- [17] M. Smidman, M. B. Salamon, H. Q. Yuan, and D. F. Agterberg, Superconductivity and spin-orbit coupling in non-centrosymmetric materials: a review, *Reports on Progress in Physics* **80**, 036501 (2017).
- [18] M. K. Kashyap and D. F. Agterberg, Vortices in cubic noncentrosymmetric superconductors, *Physical Review B* **88**, 104515 (2013).
- [19] J. Garaud, M. N. Chernodub, and D. E. Kharzeev, Vortices with magnetic field inversion in noncentrosymmetric superconductors, *Physical Review B* **102**, 184516 (2020).
- [20] A. Samoilenka and E. Babaev, Spiral magnetic field and bound states of vortices in noncentrosymmetric superconductors, *Physical Review B* **102**, 184517 (2020).
- [21] A. Buzdin, Direct Coupling Between Magnetism and Superconducting Current in the Josephson φ_0 Junction, *Physical Review Letters* **101**, 107005 (2008).
- [22] F. Konschelle and A. Buzdin, Magnetic Moment Manipulation by a Josephson Current, *Physical Review Letters* **102**, 017001 (2009).
- [23] M. N. Chernodub, J. Garaud, and D. E. Kharzeev, Chiral Magnetic Josephson Junction as a Base for Low-Noise Superconducting Qubits, *Universe* **8**, 657 (2022).
- [24] S. Chandrasekhar and P. C. Kendall, On Force-Free Magnetic Fields, *The Astrophysical Journal* **126**, 457 (1957).
- [25] J. B. Taylor, Relaxation of Toroidal Plasma and Generation of Reverse Magnetic Fields, *Physical Review Letters* **33**, 1139 (1974).
- [26] M. N. Rosenbluth and M. N. Bussac, MHD stability of Spheromak, *Nuclear Fusion* **19**, 489 (1979).
- [27] J. B. Taylor, Relaxation and magnetic reconnection in plasmas, *Reviews of Modern Physics* **58**, 741 (1986).
- [28] L. D. Faddeev and A. J. Niemi, Knots and particles, *Nature* **387**, 58 (1997).
- [29] E. Babaev, Dual Neutral Variables and Knot Solitons in Triplet Superconductors, *Physical Review Letters* **88**, 177002 (2002).
- [30] P. Sutcliffe, Skyrmion Knots in Frustrated Magnets, *Physical Review Letters* **118**, 247203 (2017).
- [31] F. N. Rybakov, N. S. Kiselev, A. B. Borisov, L. Döring, C. Melcher, and S. Blügel, Magnetic hopfions in solids, *APL Materials* **10**, 111113 (2022).
- [32] E. Radu and M. S. Volkov, Existence of stationary, non-radiating ring solitons in field theory: knots and vortons, *Physics Reports* **468**, 101 (2008).
- [33] R. A. Battye and P. M. Sutcliffe, Knots as Stable Soliton Solutions in a Three-Dimensional Classical Field Theory, *Physical Review Letters* **81**, 4798 (1998).
- [34] M. N. Chernodub, Free magnetized knots of parity-violating deconfined matter in heavy-ion collisions, [arXiv:1002.1473 \[nucl-th\]](https://arxiv.org/abs/1002.1473) (2010),.
- [35] K. Tuchin, Electromagnetic field and the chiral magnetic effect in the quark-gluon plasma, *Physical Review C* **91**, 064902 (2015).
- [36] Y. Hirono, D. E. Kharzeev, and Y. Yin, Self-similar inverse cascade of magnetic helicity driven by the chiral anomaly, *Physical Review D* **92**, 125031 (2015).
- [37] K. Tuchin, Excitation of Chandrasekhar-Kendall photons in quark gluon plasma by propagating ultrarelativistic quarks, *Physical Review C* **93**, 054903 (2016).

- [38] X.-l. Xia, H. Qin, and Q. Wang, Approach to Chandrasekhar-Kendall-Woltjer state in a chiral plasma, *Physical Review D* **94**, 054042 (2016).
- [39] D. F. Agterberg, Magnetolectric Effects, Helical Phases, and FFLO Phases, in *Non-Centrosymmetric Superconductors*, edited by E. Bauer and M. Sigrist (Springer Berlin Heidelberg, Berlin, Heidelberg, 2012) pp. 155–170.
- [40] P. Badica, T. Kondo, and K. Togano, Superconductivity in a New Pseudo-Binary $\text{Li}_2\text{B}(\text{Pd}_{1-x}\text{Pt}_x)_3$ ($x = 0 - 1$) Boride System, *Journal of the Physical Society of Japan* **74**, 1014 (2005).
- [41] A. B. Karki, Y. M. Xiong, I. Vekhter, D. Browne, P. W. Adams, D. P. Young, K. R. Thomas, J. Y. Chan, H. Kim, and R. Prozorov, Structure and physical properties of the noncentrosymmetric superconductor $\text{Mo}_3\text{Al}_2\text{C}$, *Physical Review B* **82**, 064512 (2010).
- [42] E. Bauer, G. Rogl, X.-Q. Chen, R. T. Khan, H. Michor, G. Hilscher, E. Royanian, K. Kumagai, D. Z. Li, Y. Y. Li, R. Podloucky, and P. Rogl, Unconventional superconducting phase in the weakly correlated noncentrosymmetric $\text{Mo}_3\text{Al}_2\text{C}$ compound, *Physical Review B* **82**, 064511 (2010).
- [43] R. Mizutani, Y. Okamoto, H. Nagaso, Y. Yamakawa, H. Takatsu, H. Kageyama, S. Kittaka, Y. Kono, T. Sakakibara, and K. Takenaka, Superconductivity in PtSbS with a Noncentrosymmetric Cubic Crystal Structure, *Journal of the Physical Society of Japan* **88**, 093709 (2019).
- [44] V. P. Mineev and K. V. Samokhin, Nonuniform states in noncentrosymmetric superconductors: Derivation of Lifshitz invariants from microscopic theory, *Physical Review B* **78**, 144503 (2008).
- [45] R. P. Kaur, D. F. Agterberg, and M. Sigrist, Helical Vortex Phase in the Noncentrosymmetric CePt_3Si , *Physical Review Letters* **94**, 137002 (2005).
- [46] M. A. Berger, Introduction to magnetic helicity, *Plasma Physics and Controlled Fusion* **41**, B167 (1999).
- [47] Note that despite the free energies of parity-breaking Ginzburg-Landau models are not always bounded from below (see Ref. [20] and also a remark in the appendix of Ref. [19]), their London limits converge to the same model (7).
- [48] S. Chandrasekhar, On Force-Free Magnetic Fields, *Proceedings of the National Academy of Sciences* **42**, 1 (1956).
- [49] R. G. Barrera, G. A. Estevez, and J. Giraldo, Vector spherical harmonics and their application to magnetostatics, *European Journal of Physics* **6**, 287 (1985).
- [50] J. D. Jackson, *Classical Electrodynamics* (Wiley, 3rd edition, 1999).
- [51] K. S. Thorne, Multipole expansions of gravitational radiation, *Reviews of Modern Physics* **52**, 299 (1980).
- [52] V. M. Dubovik and V. V. Tugushev, Toroid moments in electrodynamics and solid-state physics, *Physics Reports* **187**, 145 (1990).
- [53] N. A. Spaldin, M. Fiebig, and M. Mostovoy, The toroidal moment in condensed-matter physics and its relation to the magnetoelectric effect, *Journal of Physics: Condensed Matter* **20**, 434203 (2008).
- [54] N. Talebi, S. Guo, and P. A. van Aken, Theory and applications of toroidal moments in electrodynamics: their emergence, characteristics, and technological relevance, *Nanophotonics* **7**, 93 (2018).
- [55] A. Schenck, *Muon spin rotation spectroscopy: principles and applications in solid state physics* (A. Hilger, Bristol, 1985).
- [56] I. Kawasaki, I. Watanabe, H. Amitsuka, K. Kunimori, H. Tanida, and Y. Onuki, Superconducting Properties of Noncentrosymmetric Superconductor LaPt_3Si Studied by Muon Spin Spectroscopy, *Journal of the Physical Society of Japan* **82**, 084713 (2013).
- [57] R. P. Singh, A. D. Hillier, B. Mazidian, J. Quintanilla, J. F. Annett, D. M. Paul, G. Balakrishnan, and M. R. Lees, Detection of Time-Reversal Symmetry Breaking in the Noncentrosymmetric Superconductor Re_6Zr Using Muon-Spin Spectroscopy, *Physical Review Letters* **112**, 107002 (2014).
- [58] Despite the apparent logarithmic divergence in the small-impurity limit, $r_0 \rightarrow 0$, the dipole moments a_{10}^{χ} and a_{10}^{Ψ} do not diverge since at a constant magnetic dipole density M_0 , since the total dipole moment $M_0^d = M_0^d(r_0)$ diminishes with decreasing radius as r_0^3 , as seen in Eq. (31).
- [59] S. Stein, Addition theorems for spherical wave functions, *Quarterly of Applied Mathematics* **19**, 15 (1961).
- [60] F. W. J. Olver, D. W. Lozier, R. F. Boisvert, and C. W. Clark, eds., *NIST Handbook of Mathematical Functions* (Cambridge University Press, 2010).